RESPONSE TO 1ST REVIEWER

We would like to thanks the anonymous review for the constructive comments on our manuscript. In the following, we will answer to the referee's comments and suggestions.

The authors distinguish three zones within the upper crust related to the volume of granites forming the crust. In my opinion there is not so significative difference to need a differentiation in three zones with distinct lithology except to the north where upper crust reflectivity changes.

We correlate the changes in the signature of the reflectivity within the upper crust with known geological features, such as the limit of the Duero Basin-Central System, as well as the Carboniferous-Permian magmatic zonation of the Iberian Massif (Simancas, et al., 2013). In Figure 4 differences in reflectivity can be observed from North to South, and they seem to correlate quite well with the above mentioned features. However, differences can be subtle as in the transition from Zone II to Zone III, and probably would not be so relevant if the magmatic zonation was not defined. Nevertheless, reflectivity can be affected by the quantity of granites as they have low impedance contrast, because of their massive nature.
Given all these premises, we correlate this geological features with observations in the reflectivity profile. What can be inferred from these observations is a qualitative assessment of the quantity of granites within the upper crust. Therefore, below the CS the quantity of granites should be higher than in its surrounding areas as there is a more homogeneous seismic signature.

Accordingly, we have modified the following sentences between lines 296-306:

Accordingly, we suggest that the extension of granites in zone II can be prolonged to the N of the Central System, even though they do not outcrop as they are covered by the Duero Basin sediments. In this context, it can be stated that below the Central System the upper crust is mainly formed by granites down to 5.5 s TWT, as they are massive lithologies that do not feature sharp impedance contrasts at the scale of the sampling waves. Zone III is imaged by the upper crustal reflectivity in the Tajo Basin and further S, which depicts the seismic response of metasediments featuring vertical folds accompanied by few granites, thus providing scarce impedance contrasts visible to high-frequency waves and giving a high-amplitude but relatively low-frequency response. As a summary, it can be inferred that the seismic signature of the upper crust sampled by the CIMDEF experiment is strongly influenced by the amount of granites and overall differences between its seismic response (granitoids) and that of (meta)sedimentary rocks, being the former the source of a low-frequency homogeneous seismic signature.

Furthermore, the authors discuss the upper-lower crust limit as a Variscan detachment level. It is almost impossible to regret the role of Variscan deformation on west Iberia lithosphere but it is also important taking in mind that the Central System could uplift up to 2.5km in the last 20My (De Vicente et al., 2007) and more than 4km of vertical displacement during Alpine tectonic events. Deformation accommodation in a pop-up model may need a detachment level or a reactivation of a former detachment. De Vicente et al., 2018 discuss this problem. These discussions do not increase the quality of the paper. In my opinion discussion must be shorter and differentiate clearly Variscan and Alpine proposals.

We agree in the important role played by the pop-up and pop-down model proposed by De Vincente et al., 2007, in accommodating the vertical displacement recorded during the last 20My. However, we discuss two features that can be or cannot be related, the upper-lower crust boundary and the crust-mantle discontinuity. Our interpretation for the upper-lower crust boundary takes advantage of the knowledge southward of our study area, where a Variscan detachment appears at the same travel time as in the Alcudia and Iberseis datasets. We propose that this feature is the northward continuation of that seen in the Alcudia and Iberseis datasets.
The crust-mantle boundary here looks significantly different than what has been proposed to date and therefore, a new interpretation of this structure should be provided. In this regard, we take up the discussion of de Vicente et al., 2018, between the existence of a detachment level or simply lithospheric folding, and we explain why our data does not support neither of these hypothesis. Therefore, we propose a scenario where the crust south of the CS under-thrusts that of the CS and appears as a deep, north-dipping feature. We suggest that this is the result of the Alpine Orogeny whether the detachment level, previously explained, played any role or not (allowing the development of crustal-scale thrusts or not). We believe this discussion and the structures proposed equally explain most of the uplift of the CS and could even be the key to understand the difference in altitude between the northern Duero Basin and the southern Tajo Basin.

The figures are appropriate and correctly drawn. I would appreciate some references in figure 1. In the legend, basement (grey colour) refers to Alpine chains Variscan basement outcrops. It would be worth so indicate.

References have been included. Legend relating the grey Variscan basement has been corrected as suggested.

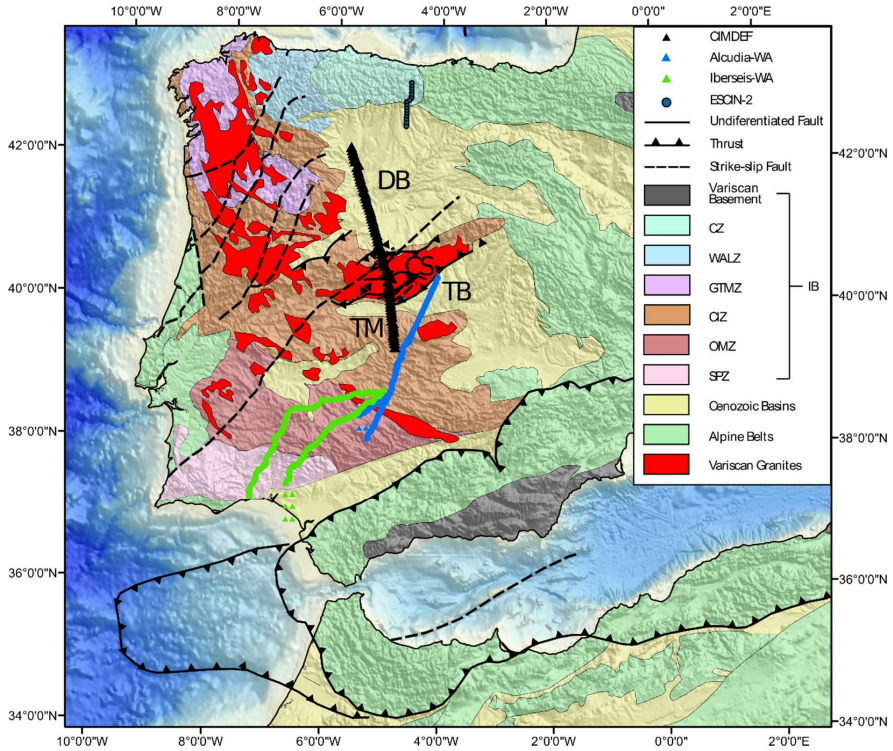

New Reference: de Vicente, G., Cunha, P. P., Muñoz-Martín, A., Cloetingh, S. A. P. L., Olaiz, A., & Vegas, R. (2018). The Spanish-Portuguese Central System: An example of intense intraplate deformation and strain partitioning. Tectonics, 37, 4444–4469. https://doi. org/10.1029/2018TC005204

The reference is already cited in line 417, but it has also been cited in other parts of the manuscript as suggested by the reviewer.

Some comments are added to the manuscript pdf

The suggestions have been included in the manuscript.

RESPONSE TO 2ND REVIEWER

We would like to thank the anonymous reviewer for the constructive comments on our manuscript. In the following, we will answer to the referee's comments and suggestions.

In general, the manuscript reads well. However, I believe that the results are over-interpreted, and there is significant potential for further improvement. In the current shape of the results, I have a hard time to associate the interpretation with the observed results in Figure 4.

First thanks for the feedback. We agree with the reviewer, there is definitely potential for further improvement, and therefore we tried to keep the interpretation to a minimum. We know that the amount of data is fairly limited and relatively sparse. The later limits the lateral resolution, which is not comparable to conventional deep wide-angle seismic reflection images. However, with this in mind, we are convinced that the few events imaged by the technique need to be relevant enough as they pop out from the data by the relatively simple processing that we have carried out. In other words, the events are there and, they, probably need to be caused by some impedance contrast (changes in Vp and density). Therefore, considering the existing knowledge of the Iberian Massif to the South and to the North of the target zone we came up with a simple model with nothing extraordinary.

For instance, the upper-lower boundary interpreted in the section is a feature seen in the Iberseis and Alcudia datasets. The proposed models constitute the northward extension of this profiles and, we think need to be consistent with the reported findings. As a result, we interpreted this feature in our model. Note that a good candidate reflection (that is, the seismic event) appears in the image at similar depth. Furthermore, similar features have been observed in other Alpine orogens (e.g. Pyrenees, Alps), and also, within the Iberian Massif, in the Cantabrian Mountains, whose origin is similar to that of the CS (Alpine reactivation of a Variscan setting).

Regarding the crust-mantle boundary, we propose an alternative model where the crust below the Tajo Basin under-thrusts that of the Central System, contrarily to what has been proposed to date, where the Moho presents a slight bulking as a consequence of lithospheric bulking as proposed by de Vicente et al. (2007, 2018). The deepening of the Moho below the Central System required by the model is a feature that has already been proposed by gravity modelling and Receiver Functions data.

Finally, we have revisited the discussion and added a few more lines and references in line 395,

These features correlate well with the results of a magnetotelluric profile carried out in the same area (Pous, et al., 2012). In their image, a zone of lower resistivity is found around the Tietar fault, which affects not only the upper crust, but extends into the lower crust, and connects even with the Moho. This low resistivity is associated with a set of faults cutting the upper crust and which could be extended to cut the whole crust although they do not need to be necessarily connected. Furthermore, preliminary results from ambient seismic noise data (Andrés et al., 2018), picture the same scenario for the crust-mantle boundary, as do new wide-angle seismic data acquired within the CIMDEF experiment, where the mid-crust discontinuity and cortical structures are clearly visible.

We thank the reviewer for the feedback, however more detailed comments would have been appreciated.

-Figure 4: The reflectivity traces can be further boosted by applying an AGC type operator. I strongly suggest that authors try this for several windows of choice.

We avoid the application of AGC as we base our interpretation in changes in the reflectivity pattern (frequency and amplitude) and applying an AGC operator would destroy amplitudes, and therefore, the signal character. Conventional automatic gain control (AGC) is applied to seismic data to bring up weak signals. Gain must be used with care, since it destroys the signal character. The resulting image has a very strong dependence on the width of the time window used and, therefore, makes strong reflections indistinguishable from weak reflections (Yilmaz 2001).

Additionally, we believed that for a sound interpretation we needed to keep the amplitude information with depth. True amplitude images are required to be certain that a reflection is due to a contrast in the physical properties (sharp change in elastic parameters).

Authors openly discuss strategies about eliminating the side lobes of the AC traces. However, in the end, they opted to use a surgical mute. It would be great if they can share their results with both of the techniques in figures.

Images of the other strategies to eliminate the side lobes have been added in the supplementary material, along with a brief explanation of each strategy.

Three different approaches were used in order to eliminate the influence of the delta pulse at time t=0 (Fig. S3).

First deconvolution of the wavelet for each station was tested. For each station the wavelet dominating the trace around t=0 s is extracted and used for deconvolution. The construction of the wavelet used the full autocorrelation stack (i.e.,

positive and negative times). The time window of the wavelet was selected by visual inspection and it was selected to be 5s. This approach did not yield good results as it suppressed most of the reflectivity throughout the profile.

The second approach is based on the subtraction of the average delta pulse. To construct the wavelet, all the stations are stacked together. The selection of the time-window to extract the wavelet followed the same procedure as in the deconvolution approach. Then the wavelet is subtracted from each station stack. This approach seems to produce similar results as the deconvolution, except it preserves more reflectivity earlier than 5 s. Still, most of the coherent reflectivity was suppressed.

The selected technique to eliminate the delta pulse was muting. We selected the time window to be muted as in the other two procedures, but to keep it as possible. A window of 3 s was selected, even though the wavelet is probably slightly longer at the southern stations compared to the northern ones. This procedure preserved the reflectivity of the profile and was selected for that reason.

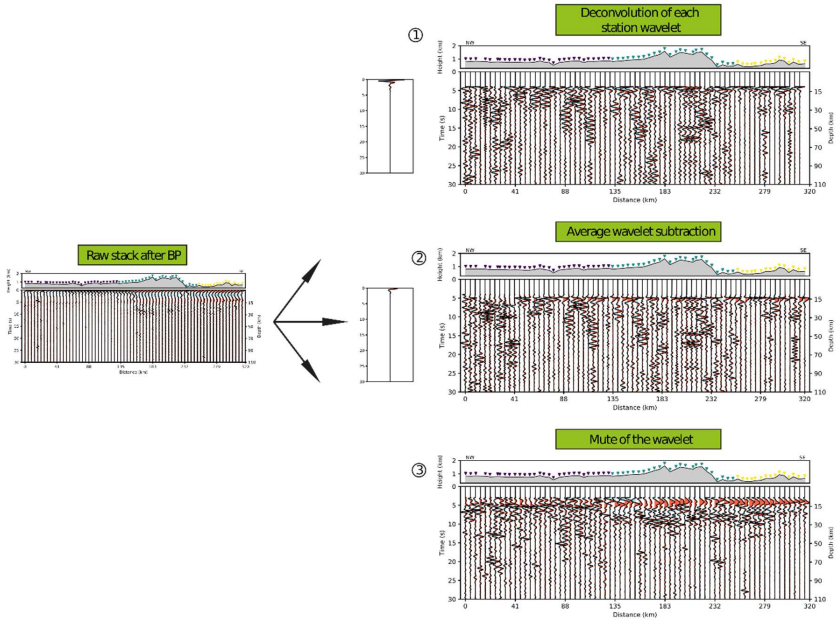

Figure S3. Approaches to eliminate the influence of the delta pulse at t=0. 1) deconvolution for each station of the wavelet, 2) subtraction of the average wavelet of all the station, 3) muting of the wavelet.

New references added:

Andrés, J., Draganov, D., Ayarza, P., Schimmel, M., Palomeras, I., Ruiz, M., Carbonell, R. Imaging the lithospheric structure of the Central Iberian Zone. EGU General Assembly, Vienna, Austria, 7-12 April 2019, EGU2019-7690, 2019.

Pous, J., Muñoz-Martín, A., Olaiz, A. J., Seillé, H., & de Vicente, G. (2012). Análisis de la estructura alpina de la corteza del centro de la Península Ibérica: Una sección Magneto-Telúrica a través del Sistema Central (Sierra de Gredos). Geo-Temas, 13, 4–8.

References

Yilmaz, O.: Seismic data analysis, Society of Exploration Geophysicists: processing, inversion and interpretation of seismic data, Society of Exploration Geophysicists, https://doi.org/10.1190/1.9781560801580, 2001.

RESPONSE TO EDITOR'S COMMENTS

We would like to thank the editor for the constructive comments on our manuscript. In the following, we will answer to the editor's comments and suggestions.

First of all, some sentences on the data quality are missing. Far distance events with 5<=M<=5.5 might contain very low energy, the authors have to state if they have made some selection among the recorded data and how; moreover, showing one example of M 5.2 is not enough, considering that its epicentral distance from the array is not mentioned. At least the authors have to show that events with M<=5.5 occurred at the largest possible epicentral distances still retain the energy necessary for this kind of analysis. The authors have to show that their data selection is the best as possible, a way of proving it is to show how the image would look like if only events with M>=6 are used.

We agree that the explanation of the data selection could be improved. We have followed the suggestions and have added more details in the form of supplementary material, as follows,

A total of 81 MW ≥ 5 earthquakes were selected for further processing. The selection of the minimum magnitude to be considered was taken as a balance between the signal quality of the earthquakes and the number of available sources for each deployment.

For each deployment, all earthquakes with MW > 5 and epicentral distance > 120° were selected. All the events within the data were checked, and the power-spectral density was computed to confirm the existence of useful energy within the selected frequency band. This process gave the final selected 81 sources.

For the first deployment a total of 44 earthquakes were analysed and 17 proved to have useful energy. In the second deployment, 59 earthquakes were evaluated, from which 38 were selected for further processing. For the final deployment, 60 earthquakes were analysed and 26 were selected to produce the final image.

For each of the three deployments a different number of earthquakes is available, 17 for the 1st, 38 for the 2nd, and 26 for the 3rd. Among those, there are 3 in the 1st deployment, 16 in the 2nd deployment and 14 for the last deployment that are with MW ≥ 6.This amount of events per deployment is insufficient for application of GloPSI. To suppress retrieval of artefacts, for example due to the PKP triplication, it is important to sum phases from a wide range of ray parameters (Ruigraok and Wapennar, 2012; Nishitsuji et al., 2016).

We have included as well a plot with the total percentages of earthquakes used in the ranges, 5 ≤ MW < 5.5, 5.5 ≤ MW < 6 and MW ≥ 6.

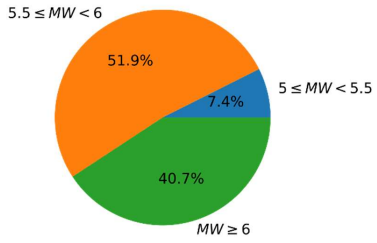

Figure S1. Percentages of events per magnitude for all used earthquakes.

Regarding the 5.2 MW event shown in Figure 3 in the manuscript, the epicentral distance is 147.1°, which, makes it the farthest 5.2 magnitude event. It is worth noting that the events, with magnitudes between 5.1 and 5.4, correspond all to the first deployment. It has been stated in the supplementary material as well.

The use of low magnitude events, between MW 5.1-5.4, is restricted to the first acquisition where the deployment time was the shorter and therefore, we were forced to include lower magnitude events in the processing scheme. These events represent the 35 % of the total events used to produce the central part of the image.

For all these reasons, we believe our data selection is good to produce a reliable lithospheric image. However, we have followed the suggestion of the editor and created an image, just of the central segment where there are only 3 earthquakes with MW ≥ 6, and compare it with our final image (we have not include it in the supplementary material).

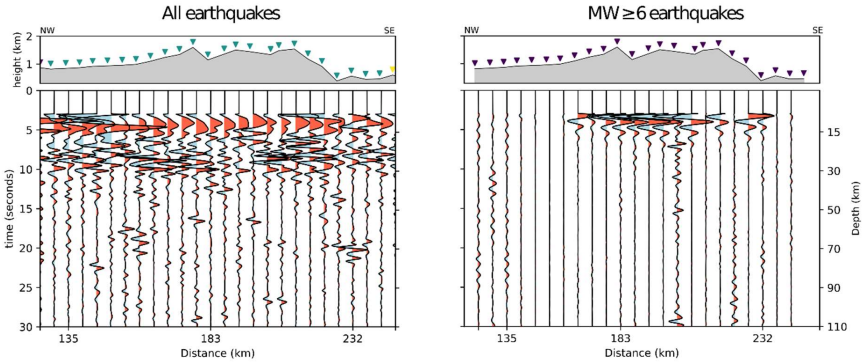

In the image with only MW ≥ 6 events, the amplitude and frequency of the autocorrelations it is clearly different, and there is small reflectivity retrieved. This could be due to a lack of information in the stacking process, or due to not retrieving the stationary phase during the stack. This would mean, that these 3 events could interfere destructively in the summation process or that the events do not cover a wide range of ray parameters, needed to produce a quality image.

Finally, we have moved the table of earthquakes presented at the end of the manuscript to the supplementary material.

Then, the several steps of how the GloPSI image has been created must be shown, in particular, the image before muting the delta pulse at t=0 and (as suggested by R2) the results after the deconvolution of the virtual source-time function and subtraction of the average time function (such image might go in the supplementary material). I would also ask how the authors are dealing with the multiple suppression, and if there are any multiples recognized in the produced image.

An image comprising all the post-stacking processing steps has been included in the supplementary material. The post-stacking process is quite straightforward as only a band-pass filter and muting of the delta pulse are applied.

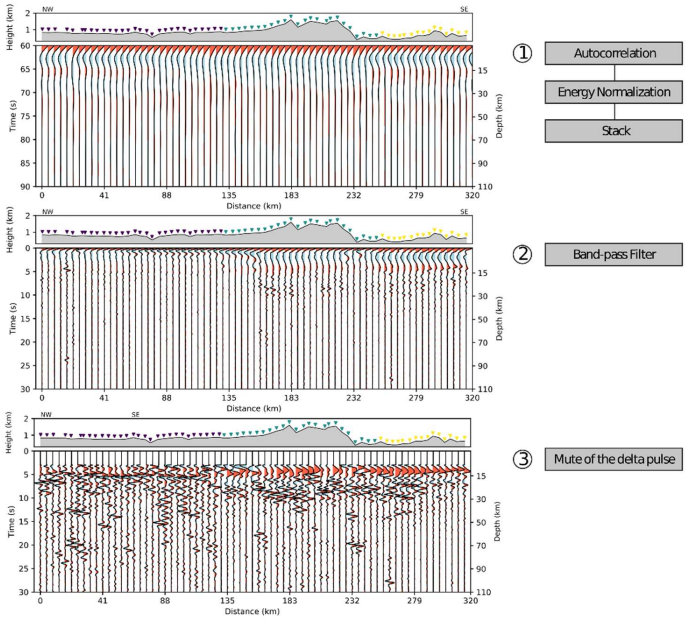

Figure S2. Stages of the processing zero-offset reflection data to construct the lithospheric image across the Spanish Central System

The following explanation has been added to the supplementary material,

The post stack processing applied to generate the zero-offset reflection profile is shown in figure S2.
Step 1 represents the raw stack of the autocorrelations of events for the three deployments, where the delta pulse around t=0 s dominates the image, as its amplitude is much higher than the amplitudes of the rest of the profile.

Step 2 comprises band-pass filtering of the raw stack to enhance higher frequencies and reject the frequencies dominated by the microseism. Therefore, a band-pass filter of 0.7-2 Hz is applied.

In step 3, the dominating delta pulse is muted. The selection of the muting window is based on the entire wavelet (including the positive and negative times of the autocorrelation). The length of the wavelet is 6 s, 3 s positive and 3 s negative times. Therefore, the muting window applied is 3 s.

We have included in the supplementary material an image comparing the three approaches to eliminate the delta pulse around t=0 s, along with a brief explanation of each strategy.

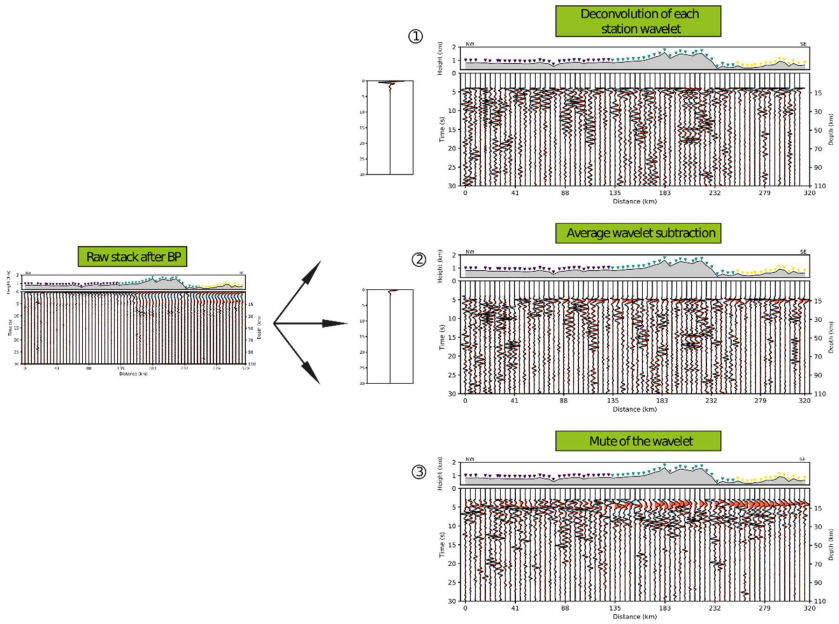

Figure S3. Approaches to eliminate the influence of the delta pulse at t=0. 1) deconvolution for each station of the wavelet, 2) subtraction of the average wavelet of all the station, 3) muting of the wavelet.

Three different approaches were used in order to eliminate the influence of the delta pulse at time t=0 (Fig. S3).

First deconvolution of the wavelet for each station was tested. For each station the wavelet dominating the trace around t=0 s is extracted and used for deconvolution. The construction of the wavelet used the full autocorrelation stack (i.e., positive and negative times). The time window of the wavelet was selected by visual inspection and it was selected to be 5s. This approach did not yield good results as it suppressed most of the reflectivity throughout the profile.

The second approach is based on the subtraction of the average delta pulse. To construct the wavelet, all the stations are stacked together. The selection of the time-window to extract the wavelet followed the same procedure as in the deconvolution approach. Then the wavelet is subtracted from each station stack. This approach seems to produce similar results as the deconvolution, except it preserves more reflectivity earlier than 5 s. Still, most of the coherent reflectivity was suppressed.

The selected technique to eliminate the delta pulse was muting. We selected the time window to be muted as in the other two procedures, but to keep it as possible. A window of 3 s was selected, even though the wavelet is probably slightly longer at the southern stations compared to the northern ones. This procedure preserved the reflectivity of the profile and was selected for that reason.

We are not applying any multiple suppression technique as we are relaying on the reflectivity patterns rather than in individual and clear reflections. Nevertheless, multiples in the image would be related to sedimentary basins, and crustal interfaces such as the upper-lower crust boundary and the Moho.

The first ones would be associated with the Duero Basin, the Tajo Basin, and the Tietar Basin. The depth of these basins is rather unknown making it difficult to apply predictive-deconvolution. Nevertheless, if we assume a depth in the range of 1-2 km depth and standard velocities for sedimentary basins of 3500 m/s, the multiples should be restricted to the upper crust. Furthermore, considering the frequencies used, the top and bottom of shallow basins could not be even resolved.

Multiples related to crustal interfaces such as the Moho should be present at times greater than 20 s. Little reflectivity is found below 20 s TWT allowing us to think that, if present, multiples are not disturbing our interpretation.

I understand that the main argument for discerning between crust and mantle is the different reflectivity of the two, while concerning the boundary between upper and lower crust the authors are referring to the different wavelength of the reflections. Honestly, as a not-expert eye, the choice of which of the reflectors has been interpreted seems arbitrary. The different amplitudes might be due to the different events used for imaging the three segments of the profiles. The authors have to clearly show that what they interpret is not an artifact but rather a robust feature, moreover the authors have to show clearly if they have used prior information on the local structure for their interpretation.

As we state in the manuscript, the interpretation is based on changes in reflectivity. We also state that we base our model with previous knowledge of the area and surrounding areas, and therefore, none of the proposed features is completely new, or to some instance random.

The boundary between the upper and lower crust is evidenced by a drastic change in the reflectivity pattern between the upper and lower crust where the frequency content and amplitudes clearly changes. This interpretation is supported by the fact that normal-incidence and wide-angle seismic data within the Iberian Massif reveal the same feature to the south of the profile, in the ALCUDIA dataset. In fact, in the crossing point between the presented dataset with the Alcudia-WA dataset, both mid-crustal interfaces appear at the same, travel time. So we suggest that the boundary we see at mid-crustal depths is the northward continuation of a feature seen along 600 km to the S of our area of study. The discontinuity can be seen in Martínez-Poyatos et al. (2012), and how it extends southwards in Simancas, et al. (2013).

Regarding the difference in amplitudes, one of the steps in our processing workflow was to normalize by their energy the autocorrelations before stacking, which make the final stacks not to be affected by different amplitude of the events.

Finally, there are several interpreted features in the mantel (outlined by green dashed lined in Figure 5). As far as I understand the GloPSI can be applied to very long arrays, due to the fact that this method is valid for interpreting phases that are constantly recognized along the array itself; therefore, such short (in space) reflectors might be artifacts and their interpretation misleading. The authors have to show how they can distinguish between real signals and artifacts in such an image.

Identification of phases with GloPSI follow the same principles as any seismic image and, therefore, reflectivity will be retrieved whenever there is a detectable change in the physical properties of the underlying materials. Because of that, GloPSI could be applied even to single station. However, using arrays always facilitates interpretation, so having several stations close to each other is always preferred. Also, the imaging with GloPSI is conditioned by the inclination of the identified structures. If they have a high dip, they will not be interpretable by their presence, but by their absence in an image from an array of stations.

The reflections that we are seeing within the upper mantle have lengths between a few kilometres and 50 km. We correlate the depth of this reflectivity with similar features seen in wide-angle data for southern Spain (Ayarza, et al., 2010). A recent study (Palomeras et al., submitted) explores these mantle reflectors further north but still in the Iberian Massif by means of a compilation of wide-angle profiles. These authors find the same features in the mantle in the western part of the Iberian Peninsula.

We agree that the lack of control over possible artifacts should be noted, especially in connection to features of shorter lateral continuity. We have included the following lines in line 465,

However, the lack of control on possible artifacts within the upper mantle should be noted and these results should be taken carefully.

LIST OF CHANGES

- Modified a bit the wording of some paragraphs to make them more clear.
- Added paragraph in the discussion of the Moho boundary to support our model
- Modified figure 1
- Modified figure 6 b to add a fault needed to geometrically compensate our model.
- Added supplementary material
- Moved the earthquake table to supplementary material.
- Added “data availability” section.
- Modified acknowledgements

Lithospheric image of the Central Iberian Zone (Iberian Massif) using Global-Phase Seismic Interferometry

Juvenal Andrés[1,3], Deyan Draganov[2], Martin Schimmel[1], Puy Ayarza[3], Imma Palomeras[3], Mario Ruiz[1], Ramon Carbonell[1]

[1]Institut of Earth Science Jaume Almera (ICTJA), 08028, Barcelona, Spain
[2]Department of Geoscience and Engineering, Delft University of Technology, Stevinweg 1, 2628 CN Delft, The Netherlands
[3]Department of Geology, University of Salamanca, 37008, Salamanca, Spain

Correspondence to: Juvenal Andrés (jandres@ictja.csic.es)

Abstract.

The Spanish Central System is an intraplate mountain range that divides the Iberian Inner Plateau in two sectors – the northern Duero Basin and the Tajo Basin to the south. The topography of the area is highly variable with the Tajo Basin having an average altitude of 450-500 m while the Duero Basin presents a higher average altitude of 750-800 m. The Spanish Central System is characterized by a thick-skin pop-up and pop-down configuration formed by the reactivation of Variscan structures during the Alpine Orogeny. The high topography is, most probably, the response of a tectonically thickened crust that should be ~~also identified by~~the response to 1) the geometry of the Moho discontinuity 2) an imbricated crustal architecture and/or 3) the rheological properties of the lithosphere. Shedding some light about these features are the main targets of the current investigation. In this work, we present the lithospheric-scale model across this part of the Iberian Massif. We have used data from the CIMDEF project, which consists of recordings of an almost-linear array of 69 short-period seismic stations, which define a 320 km long transect. We have applied the so-called Global-Phase Seismic Interferometry. The technique uses continuous recordings of global-earthquakes (> 120º epicentral distance) to extract global phases and their reverberations within the lithosphere. The processing provides an approximation of the zero-offset reflection response of a single station to a vertical source, sending (near) vertical seismic energy. Results indeed reveal a clear thickening of the crust below the Central System resulting, most probably, from an imbrication of the lower crust. Accordingly, the crust-mantle boundary is mapped as a relative flat interface at approximately 10 s two-way travel time except in the Central System, where this feature deepens towards the NW reaching more than 12 s. The boundary between the upper and lower crust is well defined and is found at 5 s two-way travel time. The upper crust has a very distinctive signature depending on the region. Reflectivity at upper-mantle depths is scattered throughout the profile, located between 13-18 s, and probably related with the Hales discontinuity.

Introduction

The Spanish Central System represents the most prominent topographic feature in Central Iberia. It is bounded by two major Tertiary – basins, namely the Duero Basin to the N and the Tajo Basin to the S, forming the Central Meseta. This mountain range extends in NE-SW direction for over 300 km, with peaks more than 2500 m in height, and is actively increasing its elevation in the order of 1mm/yr (Cloetingh et al., 2002), while the Central Meseta features an average altitude of 600-700 m.

The average elevation of the central Iberian Peninsula is the highest among those in the European continent. Current interest of Solid Earth Sciences~~,~~ is focusing towards constraining and understanding topography as a whole, its changes

and their causes. Changes in topography are the expression of the characteristics of the lithosphere and processes that affect it: 1) on the surface (such as erosion and, therefore, climate), 2) within the lithosphere itself (such as intrusion of volcanics and magmas, faulting, rifting, compression, extension etc.), and 3) corresponding isostatic rebounds. How the crust responds to these processes is mostly controlled by its internal architecture and the distribution of its physical properties. Since the early 1990s, a number of multidisciplinary geophysical studies have been undertaken to characterize the crust and lithosphere in the Iberian Massif, first to the NW, and then to the SW, up to and across the ~~Montes de~~ Toledo Mountains. Detailed crustal and, sometimes, lithospheric structures have been delineated primarily from high-resolution controlled-source (normal-incidence and wide-angle) seismic reflection/refraction data (Pulgar, et al., 1995; Ayarza et al., 1998; Simancas et al., 2003; Carbonell et al., 2004a; Flecha et al., 2009; Palomeras et al., 2009, 2011; Martínez-Poyatos et al., 2012; Ehsan et al., 2014; 2015). However, there is a gap of seismic information at the Central System and surrounding basins.

Due to its usefulness, seismic interferometry (SI) has lately consolidated itself as a tool for lithospheric imaging. Recent studies have exploited earthquakes/moonquakes recordings (Ruigrok and Wapennar, 2012; Nishitsuji et al., 2016 a,b) to image lithospheric discontinuities such as the Moho (in the Earth and the Moon) or subducting slabs. These studies are based on a technique called Global-Phase Seismic Interferometry (GloPSI) (Ruigrok and Wapennar, 2012). GloPSI is a technique that retrieves P-wave reflectivity, coming from distant energy sources, below a single station by autocorrelating earthquake phases coming nearly as a plane wave with (near) vertical incidence angles. We have employed this technique in an almost linear array of 320 km length crossing the Central System and the Duero and Tajo Basins within the Central Iberian Zone. The resulting image provides new insights on the lithospheric structure of this intraplate mountain range which complement previous results.

Our interpretations are supported by models deduced from other nearby seismic datasets available. The results from normal incidence seismic profiles ESCIN-2, IBERSEIS-NI and ALCUDIA-NI (Pulgar, et al., 1995; Simancas, et al., 2003; Martínez-Poyatos et al., 2012) as well as the velocity information provided by from the wide-angle datasets acquired as part of those experiments (e.g. IBERSEIS-WA and ALCUDIA-WA, Palomeras et al., 2009; Ehsan et al., 2015) are evaluated in our interpretation.

This work aims to contribute to the knowledge on the lithospheric structure and crustal thickness across the Central System, and to its relationship with the contrasting topography of the Duero Basin and Tajo Basin, constraints that are an asset to study the origin and evolution of the elevation and the deformation dynamics of the Iberian Peninsula.

Geological Setting

In the Iberian Massif (Fig.1) outcrops part of the Late Palaeozoic Variscan/Alleghanian Orogen of Europe. The latter was formed by the collision between pre-Mesozoic Laurentia/Baltica and Gondwana continents. The orogeny took place in two steps: 1) from Ordovician to Devonian times with the closure of the Rheic Ocean, that separated the continents, and 2) from Devonian to Carboniferous times where the continents where amalgamated along with other minor pieces like Armorica (Franke, 2000; Matte, 2001). The Iberian Massif exposes a complete section of the Variscan Belt formed by six units. External parts of the orogen are represented by the South Portuguese Zone (SPZ) to the S and the Cantabrian Zone (CZ) in the N, whereas the internal zones are the Ossa-Morena Zone (OMZ), Galicia-Tras-os-Montes Zone (GTMZ), Central Iberian Zone (CIZ), Galicia-Tras-os-Montes Zone (GTMZ), and West-Asturian Leonese Zone (WALZ) (Julivert, et al., 1972). From these domains, the CIZ, WALZ, and CZ represent continental portions of a passive margin along

Gondwana before the Variscan orogeny. Overlying the CIZ, the GTMZ is a relic of the Rheic Ocean formed partly by ophiolites. The OMZ is interpreted as a ribbon continental domain that drifted to some extent from Gondwana. Finally, the SPZ is interpreted as a fragment of Avalonia (Fonseca and Ribeiro, 1993; Tait el al., 2000).

The CIMDEF seismic profile is located within the CIZ although, the latter is overlain by Cenozoic basins to the N and S of the profile. The CIZ is the largest subdivision of the Iberian Massif and has two distinct zones (Díez Balda et al., 1990). To the N it is characterized by high-grade metamorphism and high deformation (Barbero and Villaseca, 2000) and a vast volume of Carboniferous granites~~, most of them outcropping~~ (Bea et al., 2004). The southern part is characterized by less deformed rocks, featuring NW-SE trending upright folds and faults, and a much more moderate volume of granites.

The profile crosses three main geological domains within Central Iberia, namely the Central System, the Duero and Tajo Basins. The Central System is an intraplate mountain range characterized by a thick-skin pop-up and pop-down configuration with an E-W to NE-SW orientation. It was formed during the Cenozoic Alpine compression of the Iberian Peninsula and is composed by uplifted Variscan basement (Vegas et al., 1990., de Vicente et al., 1996, de Vicente et al., 2007, de Vicente et al., 2018). It is divided into two major areas by a set of almost N-S faults. The western sector is called Gredos and the eastern side is Guadarrama-Somosierra. The outcropping materials are mainly Variscan ~~granitites~~ granitoids in the western sector with minor outcrops of metamorphic rocks, while the eastern zone is mainly composed by metamorphic rocks with minor outcropping granites. The granites of the western sector correspond to the Avila Batholith which is a vast association of igneous rocks. The current knowledge of the crustal and lithospheric structure of the Central System comes mainly from geophysical studies such as seismic data (Suriñach and Vegas, 1988, Diaz et al., 2016) and inversion and forward modelling of potential-field data (Tejero et al., 1996; De Vicente, et al., 2007; Torne et al., 2015). These studies have found a crustal thickness in the range of 31 km to 35 km, showing a thickening underneath the Central System with respect to the surrounding basins. Our study area is located in the western part of the Central System, i.e. the Gredos sector. Its structure corresponds to a main pop-up of about 100 km across the strike which can be subdivided in four short-wavelength pop-ups, of about 10-20 km, and three pop-downs framed into the pop-ups. The Duero Basin corresponds to the foreland basin of the Cantabrian Mountains to the N as well as the foreland basin of the Central System to the S. The Tajo Basin is located to the S of the Central System and the contact between them is marked by a thick-skinned thrust fault that fades out to the W. Approximately at the longitude of the CIMDEF profile, this thrust fault is substituted by a set of faults located slightly to the N and hosting the Tietar river (Fig. 2 in De Vicente et al. 2007).

The CIMDEF experiment

The data used in this study were acquired within the CIMDEF project. The set-up consisted of a three-stage deployment. The first part of the profile was recorded between May and June 2017 by 24 short-period stations equipped with 2-Hz three-component geophones. The second stage was acquired between February and April 2018 and consisted in a deployment of 15 stations, while the third deployment was undertaken between July and September 2018 and 30 new stations were installed using the same configuration of geophones and data-loggers for all deployment stages. The data were acquired in continuous recording at 250 samples per second (sps) during periods ranging from 28 to 60 days. The stations were installed along an almost linear NW-SE array with an average interstation spacing of 4.8 km, covering a total length of 320 km (Fig. 1). For every station, at least 28 days of continuous recording is available although in the northern and southern part of the profile, almost two months of data are available. For the processing, we select the vertical-component of global earthquakes (Fig. 2) with MW $\geq$ 5 from the USGS catalogue. The limited deployment time of the experiment determined the choice of MW $\geq$ 5 in order to allow the use of more sources. A total of 81 earthquakes

were selected (Table 1): 17 for the central deployment, 38 for the southern segment and 26 for the northern part of the profile.

The selection of the beginning of the time window to be used was based on the theoretical travel time of the phases calculated by the ak135 model (Kennett et al., 1995). We visually inspected the recordings and selected phases with a high signal-to-noise ratio. The time-window is set to start 30 s before the onset of specific phases of interest (e.g., PKiKP or PKIKP) and to end 300 s after the onset and before the onset of the first S-wave phase.

Global-Phase Seismic Interferometry

The GloPSI technique uses body-wave global phases that have travelled through the core and whose energy arrives at the surface nearly vertical. These seismic phases are PKP, PKiKP, and PKIKP, produced by earthquakes at >120º of epicentral distance (Fig. 2). When arriving at the station, the phases and their reverberations in the lithosphere are used as the input data. In general, these arrivals are nearly plane waves in the mantle and have a slowness lower than 0.04 s/km.

The reflections produced by the phases and their reverberations can be retrieved using SI. The methodology is based on the 1D derivation for an acoustic medium of Claerbout (1968) where reflectivity is retrieved by autocorrelation. This theory was latter extended to 3D inhomogeneous media by Wapenaar (2003) and adapted to retrieve body-waves from global earthquakes by Ruigrok and Wapenaar (2012). The GloPSI technique relies on the application of autocorrelation of every earthquake and stack over sources to retrieve the pseudo zero-offset reflections response below a station from a virtual source that radiates energy nearly vertically down. Stacking over the correct illumination range ensures cancelation of spurious events and enhancement of stationary events. Thus, we calculated the back azimuths of the selected events (inset in Fig. 2). Despite the constraint that the distance > 120º implies in terms of availability of sources, the illumination is well covered, thus ensuring a good stacking of the resulting autocorrelations. Limitations of the methodology are related with earthquake distribution and quantity and with the internal structure of the crust. As GloPSI uses nearly vertical incident energy, reverberations from steep dipping structures below the station would not be retrieved. However, the lack of imaged reflectivity of such structures can be used to interpret their presence (Nishitsuji et al., 2016a). The methodology is extensively covered in Ruigrok and Wapenaar (2012), therefore the reader is referred to the paper for further details.

Data Processing

The methodology we employ for the processing of the earthquakes recording includes pre-processing and construction of stacked autocorrelograms of the vertical component. We base our processing steps on linear autocorrelations and phase-weighted stacks (tf-PWS) (Schimmel and Gallart, 2007). The tf-PWS is based on the non-linear theory where the linear stack is weighted by the time-frequency phase. This procedure enhances coherent signals independently of their amplitudes. The time-frequency phase stack is written as

$$c_{ps}(\tau, f) = \left| \frac{1}{N} \sum_{j=1}^{N} \frac{S_j(\tau, f) e^{i2\pi f \tau}}{|S_j(\tau, f)|} \right|^{v} \quad (1)$$

where $c_{ps}(\tau, f)$ is the time-frequency phase coherence, and $S_j(\tau, f)$ is the S-transform. Then, the tf-PWS is calculated by multiplying the phase stack with the S-transform of the linear stack as,

$$S_{pws}(\tau, f) = c_{ps}(\tau, f) S_{ls}(\tau, f). \quad (2)$$

Finally, the inverse S-transform is applied to convert the stack from the frequency domain to the time domain.

The pre-processing applied to all selected time-windows consists in first, deconvolving the instrument response from the signal. Then, the data is decimated from 250 sps to 50 sps in order to reduce computing time. The next step consists in band-pass filter the data to restrict the frequency bands to those where we expect the target information to be found. We applied a broad band-pass filter of 0.1-2 Hz after computing the power-spectral density for different magnitude earthquakes (Fig. 3). Subsequently, we apply SI by autocorrelation to each selected phase (transient source). To help the correct stacking, the autocorrelations are normalized by their energy. This step aids the summation process as each phase could have a different spectral balance, thus hindering an optimal stacking. The resulting stack is filtered between 0.7-2 Hz as low frequencies offer low resolution and they (< 0.7 Hz) are influenced strongly by the microseismic noise (Fig 4).

As a consequence of the autocorrelation process, a strong arrival at t = 0 is created, representing a smeared Dirac delta function at time 0 s (Claerbout 1968; Wapenaar, 2003), dominating the earlier part of the trace. Two methodologies have been tested to reduce this effect: a) deconvolution of the wavelet around 0 t (the virtual-source time function) extracted from the average of all autocorrelations per event and phase; b) subtracting the average time function of all the traces from every individual autocorrelation. Both processes partly helped to eliminate the influence of the virtual-source time function but did not deliver optimal results. For the sake of the interpretation, we have preferred to mute the virtual-source time function, as the previous mentioned techniques have not been entirely successful.

The entire processing workflow of the earthquake recordings yields a pseudo zero-offset section with the reflection response of the lithospheric structure below all stations (Fig.4). Further post-processing steps, as elevation correction, have been considered but discarded. The maximum elevation difference in the area is approximately 1 km, that assuming an average crustal P-wave velocity of 5.5 km/s, would represent a time shift of 0.36 s, which would not modify the possible interpretation of reflectors at lithospheric scale.

Results

We present a P-wave reflectivity profile obtained by stacking autocorrelograms from phases of global earthquakes (Fig. 4). The section crosses, from NW to SE the Duero Basin (DB), Central System (CS), Tajo Basin (TB), and also the Toledo Mountains in the Central Iberian Zone (CIZ) (Fig. 1), and can be regarded as an image of the reflectivity of the upper lithosphere down to 30 s two-way travel time (TWT).

We have applied a time-to-depth conversion to display the estimated depth at which we obtain reflectors. The conversion is applied to the time axis to the left and is displayed on the right axis of Figure 4, but the velocity model is not too certain, thus the depth serves only as a reference. This conversion uses the velocity profile of shot 3 from the ALCUDIA-WA experiment, down to Moho depths, (Ehsan et al., 2015) which is fairly close to the southern end of our profile but at an offset of around 20 km (see Fig. 1). Below the Moho, a constant velocity of 8 km/s has been used in the conversion. In areas with a sedimentary cover as the Duero Basin in the northern part of the profile, the depth conversion might not be accurate because of the lower velocity in sediments, thus overestimating the real reflector depths. In addition, in areas where the crust is thicker, the resulting depth would also be overestimated as we might have used mantle velocities in crustal areas.

The relative long distance covered by the profile and the relatively close station spacing (≈ 4,8 km) ensure a high lateral resolution of the lithospheric structure of the study area. The section shown in Figure 4 shows alternating bands of high

and low reflectivity and also distinct areas of high and low frequency. The most conspicuous observations are: 1) a high-reflectivity band from the surface down to 9.5-12 s TWT, with much lower reflectivity below; and 2) another band of high-amplitude and low-frequency arrivals in the southern half of the profile above 5.5 s TWT. This band continues to the N with slightly higher frequency and lesser amplitude arrivals that are a slightly shallower. Also, apparently random reflectivity appears below 12 s TWT.

The first of the above mentioned reflective layers represents the highly reflective continental crust which can be easily separated from a more transparent mantle in this part of the CIZ and is one of the keys to calculate the crustal thickness. Among the reflectors found within the crust, a marked package of arrivals is found between 3 and 5.5 s TWT throughout the profile. This displays an almost flat structure underneath the Central System, while thinning towards the N and S of the profile. As seen in the wiggle image in Figure 4, this shallower band of reflectivity presents a different signature in the three domains, the Central System, the Tajo Basin and the Duero Basin, displaying much lower frequencies in the Central System. Accordingly, to the N and S, the ~~reflector~~ reflectivity band is defined by higher-frequency wiggles, which become very coherent to the S. Moreover, in the first 70 km of the profile this band of reflectivity features lower amplitudes and exhibits less continuity while showing a similar waveform to the wiggles further S. The bottom of this thick band of reflectivity defines a discontinuity at an average depth of 5.5 s TWT. Based on the characteristics of this feature, we can state that this discontinuity is shallower, sharper, and better defined in the northern and southern parts of the profile, although it covers the entire section. We interpret this discontinuity as the upper crust-lower crust boundary. Thus, the upper crust features a homogeneous (low frequency) signature in the Central System and is probably thinner and more heterogeneous to the N and S.

The lower crust features a high and heterogeneous reflectivity that is interpreted as the seismic expression of a laminated layer, as seen in the ALCUDIA-NI experiment (Martínez-Poyatos et al., 2012; Ehsan et al, 2014). Within this lower band of reflectivity, differences also exist between the central-southern part and the northern sector. Below the Duero Basin, a less reflective lower crust exists up to 135 km of distance, while below the Tajo Basin and the Central System, the reflections have higher amplitudes overall indicating higher impedance contrasts in that area and a coherent response regardless of the differences at upper crustal levels.

The crust-mantle discontinuity is marked by a transition from high-amplitude reflections to a much lower-amplitude seismic signature; it is difficult to define a sharp Moho discontinuity with this dataset. This transition features an increase in seismic impedance and is located between 9.5-12 s TWT (peak wiggles in Fig. 4). The Moho is shallower and more difficult to define in the northern sector where it appears slightly above 10 s. It seems rather flat until it starts deepening to the SE, at 120 km distance to the N of the Central System. Below the Central System a clear step is found, differentiating the crust-mantle boundary in two parts. From the north, the gentle deepening continues until 180 km distance, just below the northern edge of the Central System. At this point, the deepest Moho position is found below the highest elevation of the mountain range, where two traces show high-amplitude reflectivity at 12 s TWT. The Moho shallows again southwards until 230 km distance, where it becomes almost flat again, featuring depths of 10 s TWT until the end of the profile.

As expected, the mantle is more transparent than the crust and reflections are scattered and less abundant. In general, the northern sector is characterized by slightly higher reflectivity than the central and southern area. A reflection at 13-14 s

TWT is visible at different places along the profile. It features higher amplitudes under the northern part of the Duero Basin, then fading away and being visible again at 50 km, and along an interval between 80 and 110 km distance. This reflector might continue below the Central System with two conspicuous reflections at 16 s. The reflector can be followed up again below the Tajo Basin and Toledo Mountains where it gradually shallows from 14 to 13 s TWT. Below this interface, another discontinuous reflector is found between 19-20 s TWT. As before, this feature is more visible under the Duero Basin and only clear again at a distance of 230 km. At latter times, there are no clear arrivals with high enough continuity as to define a reflector (Fig. 4).

Discussion

In this work, we present the first reflectivity profile of the lithosphere under the Central Iberian Zone, in the Iberian Massif, by means of SI applied to global-earthquake data. The resulting image (Fig. 5) provides key insights to understand the internal structure and tectonic evolution of the Central System and the surrounding sedimentary basins. In the following sections, we analyse and address the nature and geometry of the crust and mantle reflectors and their possible origin. Our interpretation approach relies on the identification of arrivals which have lateral coherence, along with similar waveforms. In general terms, good lateral reflectivity is retrieved along the profile where clear crustal reflectors can be identified. Although in this work we use low-frequency global phases, the crust can be divided in upper and lower crust, both coinciding with the main reflectivity zones seen in the ALCUDIA-NI profile, which uses a higher-frequency data set (8-80 Hz). The upper crust extends from 0 to 5.5 s TWT in average (0-15 km), while the lower crust goes down to 9.5-12 s TWT (29-38 km). Therefore, two crustal-scale discontinuities are identifiable: the base of the upper crust at 5-5.5 s TWT and the crustal-mantle discontinuity between 9.5 and 12.5 s TWT. Finally, the lithospheric mantle covers the rest of the profile from depths of 29-39 km and also features two discontinuities at 13-14 s TWT and around 19-20 s TWT.

Upper Crust

The upper crust observed as part of the CIMDEF experiment (Fig. 5) is identified between 3-5.5 s TWT (7-15 km) and is characterized by a package of reflectivity with high-amplitude events and, in places, rather low frequencies. However, this package shows some differences along the profile. Below the Duero Basin two different types of reflectivity are found. From 0 to 70 km distance, relatively low-amplitude reflectivity with higher frequencies is observed. Then, higher amplitudes appear up to the Central System location. There, the reflectivity has much lower frequencies and even higher amplitudes. The signature changes again below the Tajo Basin and the Toledo Mountains where higher frequencies are present again and high amplitudes are exhibited. These ~~differences~~ changes in ~~the~~ reflectivity do not coincide with the areas surveyed in each one of the three deployments and therefore, could be attributed to lithological changes associated to the outcropping geology.

The upper crustal image observed in this section allows us to establish a correlation between the reflectivity signatures and the Carboniferous-Permian magmatic zonation of the Iberian Massif (Simancas et al., 2013). According to these authors, the magmatism in the Iberian Varsicides can be divided in four areas depending on its characteristics. From N to S, the CIMDEF profile crosses zones I, II, and III. Zone I includes the Cantabrian and Asturian-Leonese zones, is characterized by a negligible volume of post-orogenic granitoids; and corresponds to the first 70 km of the profile. Zone II has large volumes of Carboniferous granitoids (Bea, 2004) related to recycled metasediments from the continental crust (Villaseca et al., 1998, Bea et al., 2003). In this context, crustal thickening and extension has been proposed to support the high production of granites (Pérez-Estaún et al., 1991; Martínez Catalán et al., 2014). This area is crosscut by some

~~220~~ 170 km of the profile. The final zone intersected by the experiment, has much less abundant granitoids than the previous zone and represents the last 80 km of the southern end of the profile. The boundary between zones I and II coincides with a reflectivity change at upper crustal level in our profile, as the first 70 km feature a lower-amplitude signature, more heterogeneous reflectivity and higher-frequency events than the rest of the profile. Within zone II, another change of signature is found around 140 km distance, where a high-frequency/high-amplitude reflectivity is followed by a ~~low~~high-amplitude/~~high~~low-frequency reflectivity. This transition lies slightly to the N of the contact between the Tertiary sediments of the Duero Basin and the outcropping granitoids of the Central System. Despite our profile cannot constrain the uppermost part of the upper crust, the relationship between surface geology and our results is evident, and we assume that the main contacts observed at the surface are at the same locations as observed here at 3 s TWT (8-9 km). Accordingly, we suggest that the extension of granites in zone II can be prolonged to the N of the Central System, even though they do not outcrop as they are covered by the Duero Basin sediments. In this context, it can be stated that below the Central System the upper crust is ~~completely~~ mainly formed by granites down to 5.5 s TWT, as they are massive lithologies that do not feature sharp impedance contrasts at the scale of the sampling waves. Zone III is imaged by the upper crustal reflectivity in the Tajo Basin and further S, which depicts the seismic response of metasediments featuring vertical folds accompanied by few granites, thus providing scarce impedance contrasts visible to high-frequency waves and giving a high-amplitude but relatively low-frequency response. As a summary, it can be inferred that the seismic signature of the upper crust sampled by the CIMDEF experiment is strongly influenced by the amount of granites and overall differences between ~~the~~ its seismic response of igneous (granitoids) rocks and that of (meta)sedimentary rocks, being the former the source of a low-frequency homogeneous seismic signature.

Lower Crust

Below the upper crust, the CIMDEF experiment, shows a highly reflective lower crust along most of the central segment. However, lower amplitude reflectivity is found in the first 130 km to the N. Also, from the southern border of the Central System to the end of the profile, amplitudes at a lower-crustal level are somehow lower than underneath the Central System.

Although GloPSI has low resolution when compared to ~~the~~ active-source vertical-incidence reflection data, a similar reflective pattern is again identified between both types of datasets. The lower limit of the upper crust correlates well with a mid-crustal discontinuity identified in the IBERSEIS-NI and ALCUDIA-NI datasets to the S (Simancas et al., 2003: Poyatos et al., 2012; Ehsan et al., 2014) and also found in the ESCIN-2 and ESCIN-3.3 profiles to the N (Pulgar et al., 1996; Ayarza et al., 1998). This interface is present from the SPZ, the OMZ, and the southern part of the CIZ as well as in the WALZ and in the northern border between the Duero Basin and the Cantabrian Mountains. It has been regarded as the Variscan brittle/ductile transition (Simancas, et al., 2003; Palomeras, et al., 2009; Martínez-Poyatos, et al., 2012; Ehsan, et al., 2015) although ductile Variscan deformation is widespread at outcrop level in these areas, i.e. in what is supposed to be the fragile part of the Variscan crust. From a seismic point of view, this interface characterizes the division between the top of a highly laminated lower crust and a more transparent upper crust. Furthermore, this boundary separates areas with different patterns of deformation suggesting that the former might act as a detachment. Estimations of shortening at upper- and lower-crust levels, suggest that this detachment might have accommodated most of the deformation (Martínez-Poyatos, et al., 2012; Simancas et al., 2013) although these estimations fail to control the amount of ductile deformation and the part of the latter maybe previous to the Variscan Orogeny at lower crustal level.

As in the previous datasets, in the CIMDEF profile this boundary is not identifiable by a marked reflection but rather by a change in the reflectivity signature between the upper crust and the lower crust. In our profile (Fig. 5), we have also imaged how this interface continues to the north at approximately the same depth (5 s TWT). The existence of this discontinuity, that represents a boundary between layers with different deformation patterns, indicates that the upper and lower crust should have had some degree of decoupling during its tectonic evolution. If this boundary were Variscan in age, its original position could have been modified by the late Variscan igneous activity affecting the CIZ, mostly the Central System area. This may be the reason why it appears slightly deeper in the central part of the profile. In the southern border of the CS, this interface could be continuous, but also could be imbricated as an effect of the shortening, as imaged in Figures 5 and 6. Below the southern border of the CS, there is a small area where the high-reflectivity pattern of the lower crust seems to be above that of the upper crust thus suggesting the existence of this imbrication. Nevertheless, to confirm this feature, higher-resolution studies are needed.

~~There are evidences of~~Variscan orogenic evolution led to a thickening of the crust in the central and northern part of the CIZ during Carboniferous times. This ~~led to the late~~triggered extension and widespread magmatism (Pérez-Estaún et al., 1991; Díez Balda et al., 1995, Martínez-Poyatos, et al., 2012) during late Carboniferous and early Permian times~~ and to widespread magmatism~~. The presence of high-frequency reflections at lower crustal levels below the Central System evidence that here, not all the crust melted during the Variscan Orogeny in that zone. Massive granitoids do not produce reflections but rather a transparent low-frequency response. We infer then, that the lower crust below the Central System was not entirely affected by crustal melting as intense reflectivity remains. Northwards, below the Duero Basin, the lower crust is less reflective. To explain this difference, ~~two~~ three scenarios could be invoked. First, the presence of a partly melted lower crust that would imply the onset of extension and melting of the area. However, the outcropping rocks present a low metamorphic degree which is incompatible with this scenario. Second, the pre-Variscan lower crust of this area had a slightly different composition and deformation compared to its continuation to the S and N. These contrasting features might had translated in a different response to deformation during the Variscan compressional and extensional stages. Last but not least, the northern part of the CIMDEF profile lies in the Duero sedimentary basin, where Tertiary and Quaternary sedimentary layers might have absorbed part of the seismic energy thus attenuating the corresponding amplitudes. This hypothesis is supported by the fact that, in general, amplitudes are lower in the northern part of the profile.

The most prominent feature in the profile is the crust-mantle boundary (Fig. 5). The Moho topography of the Central System has been suggested, by gravity modelling (De Vicente et al., 2007) and seismic receiver functions (RF) (Mancilla & Diaz, 2015), to have a gentle bulk in a synform-like structure of long wavelength, increasing its thickness up to 2-3 km with respect to its surroundings. The crust-mantle discontinuity here is not presented as a unique and sharp reflection, but by a change in the reflectivity pattern instead. We have interpreted the discontinuity (Fig. 5) at 9.5-12 s (29-38 km), based on the position of a boundary between a highly reflective crust that passes to an upper mantle characterized by low-reflectivity and small-amplitude events. In normal-incidence seismic data, the contrast between high and low reflectivity (or transparent) has been used as the criteria to define the position of the Moho (Carbonell et al., 2013). This reflectivity boundary is irregularly distributed, being shallower to the N, around 9.5-10 s (29 km) and deepening in the central part of the profile, although shallowing again to the S. Accordingly, below the highest peak of the Central System, an overlap of two Moho branches ~~of the Moho~~ is found (Fig. 5), ~~where~~ being the deepest set of reflectors ~~is found~~ at ~~times as deep as~~ 12 s TWT (38 km). This package of reflectivity is limited to the recordings of two stations and covers a distance of ≈ 15 km, while the whole thickening covers an area of ≈100 km, going from the southern border of the Central System and

to the southern part of the Duero Basin. The fact that the presence of these deeper reflections is limited to 2 stations might not be a structural feature, but related with the methodology itself. Because GloPSI uses near vertical incident energy, it is insensible to steeply tilted structures, as the reflection of these cannot be recorded below the same station. Thus, if a steep angle is found in a structure below the Central System, our results would not recover it. Furthermore, the frequency content of such distant earthquakes is quite low, limiting the vertical resolution that can be resolved. As a consequence, other reflections shallower than those two already retrieved but deeper than the Moho, between these two and the S limit of the CS, might not be resolved with the frequency used in our study, or the signal could be mixed with that of the lower crust.

In Figure 5, we have interpreted this ~~feature~~ crustal thickening as the result of the lithospheric compression that occurred during the Alpine Orogeny, which has further modified the structure of the Variscan crust, triggering an imbrication and ~~thickening of the lower crust~~developing a crustal root that can be only partly observed with this dataset. This structure would be similar to the imbrication of lower crust identified in the Cantabrian Mountains and Pyrenees as a result of Alpine compression (Pulgar et al., 1995; Teixell et al., 2018, among others). Although in our case the observation of this underthrusting is limited by the number of recording stations, a clear thickening of the crust below the Central System can be observed anyway. The northern boundary of this crustal thickening reveals no apparent correlation with major outcropping structures. However, the southern boundary of the thickened crust lies close to the south Central System (SCS) thrust and to the fault system that defines the Tietar river basin (Fig. 6a and b). A prolongation of this lower crustal imbrication into the upper crust could project in any of these thrusts and would imply that the whole crust is in fact somehow imbricated, giving us additional insights on the origin of the low topography of the meseta to the S of the Central System (Fig. 6b). However, this would require that the identified Variscan mid-crustal detachment did not work as such during the Alpine compression (as shown in Fig. 6a), allowing compressive structures to affect both, the upper and the lower crust simultaneously. In addition, seismic profiles crosscutting the Madrid Basin and the SCS thrust to the NE of our profile (de Vicente et al., 2013), do not show underthrusting of sediments of this basin, indicating that if this tectonic feature exists, it is probably related to the Tietar River fault system.

The crustal pattern suggested above correlates well with the results of a magnetotelluric profile carried out in the same area (Pous, et al., 2012). In their image, a zone of lower resistivity is found around the Tietar fault, which affects not only the upper crust, but extends into the lower crust, and connects even with the Moho. This low resistivity is associated with a set of faults cutting the upper crust and could be extended to cut the whole crust although they do not need to be necessarily connected. Furthermore, preliminary results from ambient seismic noise data (Andrés et al., 2018), picture the same scenario for the crust-mantle boundary, as do new wide-angle seismic data acquired within the CIMDEF experiment, where the mid-crust discontinuity and cortical structures are clearly visible. In any case, the resolution of this data set does not allow us to identify steeply dipping crustal features. Higher-resolution solutions and estimations of the shortening at upper and lower crustal levels should be used to support any of these hypothesis. In any case, the structure of the CS suggested by the present dataset is that of an asymemetric orogen.

Figure 6 shows a sketch of the interpretation of the CIMDEF GloPSI profile overlapped with the Moho geometry deduced from gravity inversion (Torne et al., 2015), and a compilation of active-source and RF Moho depths (Diaz et al., 2016). Also, the geometry of the inferred imbrication, involving just the lower crust (Fig. 6a) or the upper and lower crust (Fig. 6b) is included. In general, there is a good agreement between the three models, with only small mismatches in the root area. To the S, a similar thickness of around 32-34 km is depicted from the different models. To the N, the model

presented in this paper shows a thinner crust of around 30 km while the two other models present thickness of 32-33 km. This mismatch, which is reduced along the profile towards the northern border of the CS, could be due to the existence of low-velocity sediments in the Duero Basin that lead to errors in the time to depth conversions. The differences below the CS affect the depth as well as the geometry of the crust-mantle interface. The Moho discontinuity in Diaz et al. (2016) presents a rather flat geometry, depicting a little, 1-km-thick root. The results from gravity inversion, while being closer with our results regarding crustal thickness, are highly influenced by the inclusion of the topography in the inversion procedure. Accordingly, the crustal thickening starts further to the S, showing a progressive thinning in the area where our crustal thickness is maximum. This implies that the model based on gravity inversion relates the root with local isostasy whereas our model infers a tectonic influence in the geometry and position of the crust-mantle boundary. In any case, the resolution of the datasets and the limitations of the GloPSI technique in imaging steeply dipping interfaces allows the observed small differences in the results of different techniques.

The mechanism that gives rise to the uplift and crustal thickening of the Central System is an ongoing discussion where two main hypotheses are proposed. First, several studies (Cloetingh et al., 2002; de Bruijne and Andriessen, 2002; de Vicente et al., 2007, de Vicente et al., 2018) have suggested lithospheric folding of Iberia to be the driving force. They base their hypothesis on gravity and analogue modelling, basin infill, and structural analysis of outcropping geology. They propose a model where the crust has buckled entirely, and deformation is represented in the upper crust by the formation of pop-ups that uplift the basement, while ductile deformation is present in the lower crust. The folding wavelength in continental Iberia is calculated to be between 150 to 250 km (Muñoz-Martín et al., 2010). The second hypothesis proposes that a detachment level runs from the Betics to the S or the Pyrenees to the N (Quintana et al., 2015). This solution would mean that a simple shear with a detachment at some crustal level would accommodate the shortening and provide the uplift of the Central System. Our reflectivity image provides insights that might shed some light on its structure. Despite the presence of a clear thickening under the Central System, which affects the upper crust, the lower crust is not much bulked but it seems tectonically imbricated below the Central System, thus defining and asymmetry. Furthermore, the wavelengths proposed for the lithospheric folding should be visible in our array length but contrarily. ~~Furthermore~~, the thickening of the crust under the Central System seems to be the only remarkable curvature within the crust. The second hypothesis above discussed is mainly based on the idea that the Central System has a small crustal root. This statement is based on the current geophysical knowledge of the area which includes gravity modelling (de Vicente et al., 2007), gravity inversion (Torne et al., 2015), and receiver-function studies (Mancilla & Diaz, 2015). Considering our results, the crustal root is not as small as previously seen in other geophysical datasets, and at the deepest point it might define an offset of 6-7 km. We suggest that the crustal root should have formed during the Alpine orogeny by the compression of Africa in NW direction. Consequently, we infer underthrusting or stacking/imbrication of two layers of (lower) crust as the formation mechanism. This might have accommodated much the shortening produced during the compression. If the entire crust (and not just the lower crust) were imbricated, this hypothesis could further explain the elevation difference between the Tajo and Duero Basins, as the latter is isostatically supported by a thicker crust and the former is underthrusting.

Upper mantle

The upper-mantle reflections are scattered within the profile at two main levels (Fig. 5) - between 13-14 s TWT and between 19-20 s TWT. Both reflections have low lateral continuity and, although they are visible almost throughout the entire array, the lack of continuity among patches of reflectivity hinders their interpretation and definition of their geometry. Both sets of reflectivity are nearly parallel except below the Central System, where the first reflection deepens

while the second does not. At these depths, 45-55 km for the top reflection and 70-75 km for the bottom one, other similar reflectors have been found in southern Iberia. In the IBERSEIS profile, a zone between 61 and 72 km depth was modelled, corresponding to what the authors interpreted to be the Hales discontinuity (Ayarza et al., 2010). The same discontinuity has been imaged by the ALCUDIA-WA datasets (Palomeras et al., submitted). The discontinuity, modelled by wide-angle seismic data, is proposed to be related to the mineral phase transition from spinel-lherzolite to garnet-lherzolites (Hales, 1969). To compensate for the low reflection coefficient of this phase change and to explain the thickness and high reflectivity of this feature, an area of layering or lenses with different ratios of spinel/garnet and thickness that allow constructive interferences of the seismic waves has been proposed. Moreover, to the N, below the ALCUDIA-NI profile (Martínez-Poyatos et al., 2012), conspicuous scattered reflectors are found at the same time/depth, between 13-14 and 19 s TWT. These have been interpreted to be also images of the Hales discontinuity in the area (Palomeras et al., submitted). In the same form, the reflectivity seen below the CIMDEF experiment between 45-75 km might be related to a mineral phase transition. To confirm the existence and extend of this area, velocity information would be needed. In this regard, a similar scenario is found below the Urals, where a heterogeneous upper mantle, as the one of this study, was sampled by a dense wide-angle seismic experiment (Carbonell, 2004b).

However, the lack of control on possible artifacts within the upper mantle should be noted and these results should be taken carefully.

Conclusions

In this work, we present a lithospheric scale reflectivity profile of the central part of the Iberian Peninsula by means of Global Phase Seismic Interferometry (GloPSI) acquired as part of the CIMDEF project. The array covers the Cenozoic Duero and Tajo basins, to the N and S respectively of the Central System. The most relevant finding of the resulting image is the thickening of the Central System crust through a northward directed imbrication of its lowermost part. In general, the crust-mantle boundary presents depths between 29-31 km to the N and S of the profile, while below the Central System it reaches depths of 38 km. The crustal thickening has a wavelength of around 100 km, and encloses the entire Central System, from the southern thrust, the boundary to the S with the Tajo Basin, until the southern border of the Duero Basin. As yet, it is not clear if the imaged lower crust imbrication affects also the upper crust. In fact, the surface projection of this feature could be projected on top of the southern Central System thrust or the Tietar River faults system, thus indicating that the whole crust might be affected by this feature and further explaining the low topographies of the meseta to the S of the Central System. However, the fact that a Variscan mid-crustal detachment has been inferred and the lack of estimations of lower crustal shortening hinder this interpretation. Higher resolution datasets are necessary to image these features.

Furthermore, the profile reveals a clear different reflectivity signature within the crust. The crust is subdivided into two main layers, the upper and lower crust. The upper crust is inferred to be formed mainly by massive granitoids under the Central System down to 5.5 s TWT, as its seismic response is dominated by low frequencies and high amplitudes. Below this layer, the lower crust is characterized by high frequency and high amplitude arrivals, supporting the existence of high impedance contrast layers that have been already imaged with vertical incidence data in the lower crust to the S and N of the CIMDEF profile.

The interface that separates upper and lower crust (≈12.5-15 km depth), is proposed to be a detachment level between both crusts. However, the characteristics of the outcropping rocks, showing ductile deformation in many areas hinders its

interpretation as fragile-ductile transition. Further studies about this interface are in progress and will be presented elsewhere.

Within the upper mantle, patches of reflectivity are found in two bands, 45-55 km depth and 70-75 km depth. Both reflections are scattered through the profile and appear almost flat. We relate them both with the possible N extension of the Hales discontinuity, the transition zone from spinel-lherzolite to garnet-lherzolite already observed to the S of this profile.

Author contributions.

JA, MR, IM and PA acquired the data. JA and DD processed the data. JA prepared the manuscript. All authors have contributed to the discussion and manuscript review.

Data availability

Data information is available in Labsis repository and selecting the corresponding year for each deployment. For access to the data itself, contact the Juvenal Andrés or Ramon Carbonell.

Con formato: Fuente: Sin Cursiva

Competing interests.

The authors declare that they have no conflict of interest

Acknowledgements

This study was supported by: tThe Spanish National Research Program under grants refs.: CGL2014-56548-P; CGL2016-81964-REDE; the regional government of Castilla and León by project SA065P17; the Generalitat de Catalunya 2017-SGR-1022; J. A. is supported by FPI grant BES-2015-071683 from the Spanish State Department of Science Innovation and Universities. The data used for the research carried out in this contribution is stored at the DIGITAL.CSIC data repository. We would like to acknowledge the ICTJA-CSIC Seismic Laboratory (http://labsis.ictja.csic.es/) for making their seismic station available for this experiment. The review of two anonymous reviewers and the editor

915

920

925

930 **Bibliography**

Andrés, J., Draganov, D., Ayarza, P., Schimmel, M., Palomeras, I., Ruiz, M., Carbonell, R. Imaging the lithospheric structure of the Central Iberian Zone. EGU General Assembly, Vienna, Austria, 7-12 April 2019, EGU2019-7690, 2019.

Ayarza, P., Martínez Catalán, J.R., Gallart, J., Dañobeitia, J.J., Pulgar, J.A.: Estudio Sísmico de la Corteza Ibérica Norte 3.3: A seismic image of the Variscan crust in the hinterland of the NW Iberian Massif, Tectonics, 17, 171–186, 1998.

935

Ayarza, P., Palomeras, I., Carbonell, R., Afonso, J.C., Simancas, J.F.: A wide-angle upper mantle reflector in SW Iberia: Some constraints on its nature, Physics of the Earth and Planetary Interiors ,181, 88–102, doi:10.1016/j.pepi.2010.05.004, 2010.

940 Banda, E., Suriñach, E., Aparicio, A., Sierra, J., Ruiz de la Parte, E.: Crust and upper mantle structure of the central Iberian Meseta (Spain), Geophysical Journal of the Royal Astronomical Society 67, 779–789, 1981.

Barbero, L., and Villaseca, C.: Eclogite facies relicts in metabasites from the Sierra de Guadarrama (Spanish Central System): P-T estimations for the Hercynian evolution, Mineralogical Magazine, 64, 815–836, 2000.

945

Con formato: Inglés (Reino Unido)

Con formato: Inglés (Reino Unido)

Con formato: Inglés (Reino Unido)

Con formato: Fuente: Sin Negrita

Bea, F., Montero, P., Zinger, T.: The nature, origin and thermal influence of the granite source layer of Central Iberia, The Journal of Geology, 111, 579–595, 2003.

Bea, F.: La naturaleza del magmatismo de la Zona Centroibérica: Consideraciones generales y ensayo de correlación, in Geología de España, edited by J. A. Vera, pp. 128–133, SGE-IGME, Madrid, 2004.

Carbonell, R., Simancas, F., Juhlin, C., Pous, J., Pérez-Estaún, A., González-Lodeiro, F., Muñoz, G., Heise, W., Ayarza, P.: Geophysical evidence of a mantle derived intrusion in SW Iberia, Geophysical Research Letters, 31, L11601, doi:10.1029/2004GL019684, 2004a.

Carbonell, R.: On the nature of the mantle heterogeneities and discontinuities: evidence from a very dense wide-angle shot record, Tectonophysics, 388, 103-117, 2004b.

Carbonell, R., Levander, A., Kind, R.: The Mohorovičić discontinuity beneath the continental crust: An overview of seismic constraints, Tectonophysics, 609, 353-376, doi.org/10.1016/j.tecto.2013.08.037, 2013.

Claerbout, J.: Synthesis of a layered medium from its acoustic transmission response: Geophysics, 33, 264–269, doi: 10.1190/1.1439927, 1968.

Cloetingh, S., Burov, E., Beekman, F., Andeweg, B., Andriessen, P.A.M., Garcia-Castellanos, D., de Vicente, G., Vegas, R.: Lithospheric folding in Iberia, Tectonics, 21(5), 1041, 2002.

De Bruijne, C. H., and Andriessen, P. A. M.F.: Fault related denudation in the Spanish Central System (central Spain), recording the far field effects of Alpine plate tectonic history of the Iberian microplate, Tectonophysics, 349, 161 – 184, 2002.

de Vicente, G., Giner, J.L., Muñoz-Martín, A., González-Casado, J.M., Lindo, R.: Determination of present-day stress tensor and neotectonic interval in the Spanish Central System and Madrid Basin, central Spain: Dynamics of Extensional Basins and Inversion Tectonics, Tectonophysics, 266, 405-424. doi:10.1016/S0040-1951(96)00200-4, 1996.

de Vicente, G., Vegas, R., Muñoz Martín, A., Silva, P.G., Andriessen, P., Cloetingh, S., González Casado, J.M., Van Wees, J.D., Álvarez, J., Carbó, A., Olaiz, A.: Cenozoic thick-skinned deformation and topography evolution of the Spanish Central System, Global and Planetary Change, 58, 335-381. doi:10.1016/j.gloplacha.2006.11.042, 2007.

de Vicente, G., Cunha, P. P., Muñoz-Martín, A., Cloetingh, S. A. P. L., Olaiz, A., Vegas, R.: The Spanish-Portuguese Central System: An example of intense intraplate deformation and strain partitioning, Tectonics, 37, 4444–4469. https://doi.org/10.1029/2018TC005204, 2018.

Diaz, J., Gallart, J., Carbonell, R.: Moho topography beneath the Iberian-Western Mediterranean region mapped from controlled-source and natural seismicity surveys, Tectonophysics, 692, 74-85, http://dx.doi.org/10.1016/j.tecto.2016.08.023, 2016.

Díez Balda, M. A., Vegas, R., González Lodeiro, F.: Central- Iberian Zone. Autochthonous Sequences. Structure, in Pre-Mesozoic Geology of Iberia, edited by R. D. Dallmeyer and E. Martínez García, pp. 172–188, Springer, Berlin, 1990.

Díez Balda, M. A., Martínez Catalán, J.R., Ayarza, P.: Syn-collisional extensional collapse parallel to the orogenic trend in a domain of steep tectonics: The Salamanca detachment zone (Central Iberian Zone, Spain), Journal of Structural Geology, 17, 163– 182, 1995.

Ehsan, S. A., Carbonell, R., Ayarza, P., Martí, D., Pérez-Estaún, A., Martínez-Poyatos, D., Simancas, F., Azor, A., Mansilla, L.: Crustal deformation styles along the reprocessed deep seismic reflection transect of the Central Iberian Zone (Iberian Peninsula),Tectonophysics, 621, 159–174, http://dx.doi.org/10.1016/j.tecto.2014.02.014, 2014.

Ehsan, S. A., Carbonell, R., Ayarza, P., Martí, D., Martínez-Poyatos, D., Simancas, J.F., Azor, A., Ayala, C., Torné, M., Pérez-Estaún A.: Lithospheric velocity model across the Southern Central Iberian Zone (Variscan Iberian Massif): The ALCUDIA wide-angle seismic reflection transect, Tectonics, 34, 535–554, doi:10.1002/2014TC003661, 2015.

Flecha, I., Palomeras, I., Carbonell, R., Simancas, F., Ayarza, P., Matas, J., González-Lodeiro F., Peréz-Estaún, A.: Seismic imaging and modelling of the lithosphere of SW-Iberia, Tectonophysics, 472(1–4), 148–15, doi:10.1016/j.tecto.2008.05.033, 2009.

Fonseca, P., Ribeiro, A.: Tectonics of the Beja-Acebuches Ophiolite: a major suture in the Iberian Variscan Foldbelt, Geologische Rundschau, 82(3), 440-447, https://doi.org/10.1007/BF00212408, 1993.

Franke, W.: The mid-European segment of the Variscides: tectonostratigraphic units, terrane boundaries and plate tectonic evolution, in Orogenic Processes: Quantification and Modelling in the Variscan Belt, edited by W. Franke et al., Geological Society, London, Special Publications, 179, 35–61, doi:10.1144/GSL.SP.2000.179.01.05, 2000.

Hales, A.: A seismic discontinuity in the lithosphere, Earth and Planetary Science Letters 7, 44–46, 1969.

Julivert, M., M. Fontboté, A. Ribeiro, and Conde, L. E.: Mapa y Memoria Explicativa del Mapa Tectónico de la Península Ibérica y Baleares, scale 1: 1,000,000, 113 pp., Inst. Geol. y Min. de Esp., Madrid, 1972.

Kennett B.L.N., Engdahl, E.R., Buland R.: Constraints on seismic velocities in the earth from travel times, Geophysical Journal International, 122, 108-124, 1995.

Mancilla, F.L., Diaz, J.: High resolution Moho topography map beneath Iberia and Northern Morocco from receiver function analysis, Tectonophysics, 203-211. http://dx.doi.org/10.1016/j.tecto.2015.06.017, 2015.

Martínez Catalán, J.R., Rubio Pascual, F.J., Díez Montes, A, Díez Fernández, R., Gómez Barreiro, J., Dias da Silva, I., González Clavijo, I., Ayarza, P., Alcock, J.E.: The late Variscan HT/LP metamorphic event in NW and Central Iberia: relationships to crustal thickening, extension, orocline development and crustal evolution, Geological Society, London, Special Publications, 405, https://doi.org/10.1144/SP405.1, 2014.

Martínez-Poyatos, D., Carbonell, R., Palomeras, I., Simancas, F., Ayarza, P., Martí, D., Azor, A., Jabaloy, A., González Cuadra, P., Tejero, R., Martín Parra, L.M., Matas, J., González Lodeiro, F., Pérez-Estaún, A., García Lobón, J.L., Mansilla, L.: Imaging the crustal structure of the Central Iberian Zone (Variscan Belt): the ALCUDIA deep seismic reflection transect, Tectonics 31(3), TC3017, http://dx.doi.org/10.1029/2011TC002995, 2012.

Matte, P.: The Variscan collage and orogeny (480–290 Ma) and the tectonic definition of the Amorica microplate: A review, Terra Nova, 13, 122–128, doi:10.1046/j.1365-3121.2001.00327.x, 2001.

Muñoz-Martín, A., De Vicente, G., Fernández-Lozano, J., Cloetingh, S. A. P. L., Willingshofer, E., Sokoutis, D., Beekman, F.: Spectral analysis of the gravity and elevation along the western Africa–Eurasia plate tectonic limit: Continental versus oceanic lithospheric folding signals, Tectonophysics, 495(3-4), 298–314. https://doi.org/10.1016/j.tecto.2010.09.036, 2010.

Nishitsuji, Y., E. Ruigrok, M. Gomez, K. Wapenaar, Draganov, D.: Reflection imaging of aseismic zone of the Nazca slab by global-phase seismic interferometry: Interpretation, 4, doi: 10.1190/int-2015-0225.1, 2016a.

Nishitsuji, Y., Rowe, C.A., Wapenaar, K., Draganov, D.: Reflection imaging of the Moon's interior using deep-moonquake seismic interferometry, Journal Geophysical Resarch: Planets, 121, 695–713, doi:10.1002/2015JE004975, 2016b.

Palomeras, I., Carbonell, R., Flecha, I., Simancas, F., Ayarza, P., Matas, J., Martínez-Poyatos, D., Azor, A., González Lodeiro, F., Pérez-Estaún, A.: The nature of the lithosphere across the Variscan Orogen of SW-Iberia: Dense wide-angle seismic reflection data, Journal of Geophysical Resesarch: Solid Earth, 114, B02302, doi:10.1029/2007JB005050, 2009.

Palomeras, I., Carbonell, R., Ayarza, P., Fernandez, M., Simancas, F., Martínez-Poyatos, D., González Lodeiro, F., and A. Pérez-Estaún, A.: Geophysical model of the lithospher across the Variscan Belt of SW-Iberia: multidisciplinary assessment, Tectonophysics, 508, 42–51, http://dx.doi.org/10.1016/j.tecto.2010.07.010, 2011.

Pérez Estaún, A., Martínez Catalán, J.R., Bastida, F.: Crustal thickening and deformation sequence in the footwall to the suture of the Variscan belt of northwest Spain, Tectonophysics, 191, 243–253, 1991.

Pous, J., Muñoz-Martín, A., Olaiz, A. J., Seillé, H., & de Vicente, G. (2012). Análisis de la estructura alpina de la corteza del centro de la Península Ibérica: Una sección Magneto-Telúrica a través del Sistema Central (Sierra de Gredos). Geo-Temas, 13, 4–8.

Pulgar, J. A., Pérez-Estaún, A., Gallart, J., Álvarez-Marrón, J., Gallastegui, J., Alonso, J. L., and ESCIN Group: The ESCIN-2 deep seismic reflection profile: a traverse across the Cantabrian Mountains and adjacent Duero basin, Revista Sociedad Geológica España, 8, 383–394, 1995.

Quintana, I., Pulgar, J. A., Alonso, J. L.: Displacement transfer from borders to interior of a plate: A crustal transect of Iberia, Tectonophysics, 663, 378–398. https://doi.org/10.1016/j.tecto.2015.08.046, 2015.

Código de campo cambiado

Con formato: Español (España)

Con formato: Español (España)

Ruigrok, E., Wapenaar, K.: Global-phase seismic interferometry unveils P-wave reflectivity below the Himalayas and Tibet, Geophysical Research Letters, 39, L11303, doi: 10.1029/2012GL051672, 2012.

Schimmel, M., Gallart, J.: Frequency-dependent phase coherence for noise suppression in seismic array data, Journal of Geophysical Research: Solid Earth, 112, B04303, doi:10.1029/2006JB004680, 2007.

Simancas, J.F., Carbonell, R., González Lodeiro, F., Pérez-Estaún, A., Juhlin, C., Ayarza, P., Kashubin, A., Azor, A., Martínez-Poyatos, D., Almodóvar, G.R., Pascual, E., Sáez, R., and Expósito,: Crustal structure of the transpressional Variscan orogen of SW Iberia: SW Iberia deep seismic reflection profile (IBERSEIS), Tectonics, 22(6), 1062, doi:10.1029/2002TC001479, 2003.

Simancas, J. F., Ayarza, P., Azor, A., Carbonell, R., Martínez-Poyatos, D., Pérez-Estaún, A., and González Lodeiro, F.: A seismic geotraverse across the Iberian Variscides: Orogenic shortening, collisional magmatism, and orocline development, Tectonics, 32, 417–432, doi:10.1002/tect.20035, 2013.

Suriñach, E., Vegas, R., 1988. Lateral inhomogeneities of the Hercynian crust in central Spain. Physics of the Earth and Planetary Interior, 51, 226–234.

Tait, J., Schätz, M., Bachtadse, V., Soffel, H.: Palaeomagnetism and Palaeozoic palaeogeography of Gondwana and European terranes, in Orogenic Processes: Quantification and Modelling in the Variscan Belt, edited by W. Franke et al., Geological Society, London, Special Publications, 179, 21–34, doi:10.1144/GSL.SP.2000.179.01.04, 2000.

Teixell, A., Labaume, P., Ayarza, P., Espurt, N., de Saint Blanquat, M., Lagabrielle, Y.: Crustal structure and evolution of the Pyrenean-Cantabrian belt: A review and new interpretations from recent concepts and data, Tectonophysics, 724–725, 146-170, https://doi.org/10.1016/j.tecto.2018.01.009, 2018.

Tejero, R., Perucha, M.A., Rivas, A., Bergamín, J.F.: Gravity and structural models of Spanish Central System, Geogaceta, 20, 947-950, 1996.

Torne, M., Fernàndez, M., Vergés, J., Ayala, C., Salas, M. C., Jimenez-Munt, I., Diaz, J.: Crust and mantle lithospheric structure of the Iberian Peninsula deduced from potential field modeling and thermal analysis, Tectonophysics, 663, 419–433. https://doi.org/10.1016/j.tecto.2015.06.003, 2015.

Vegas, R., Vázquez, J.T., Suriñach, E., Marcos, A.: Model of distributed deformation, block rotations and crustal thickening for the formation of the Spanish Central System, Tectonophysics, 184, 367-378. doi:10.1016/0040-1951(90)90449-I, 1990.

Villaseca, C., Barbero, L., Rogers, G.: Crustal origin of Hercynian peraluminious granitic batholiths of Central Spain: Petrological, geochemical and isotopic (Sr, Nd) arguments, Lithos, 43, 55–79, 1998.

Wapenaar, K.: Synthesis of an inhomogeneous medium from its acoustic transmission response, Geophysics, 68, 1756–1759, doi: 10.1190/1.1620649, 2003.

1115

1120

1125

1130

FIGURES

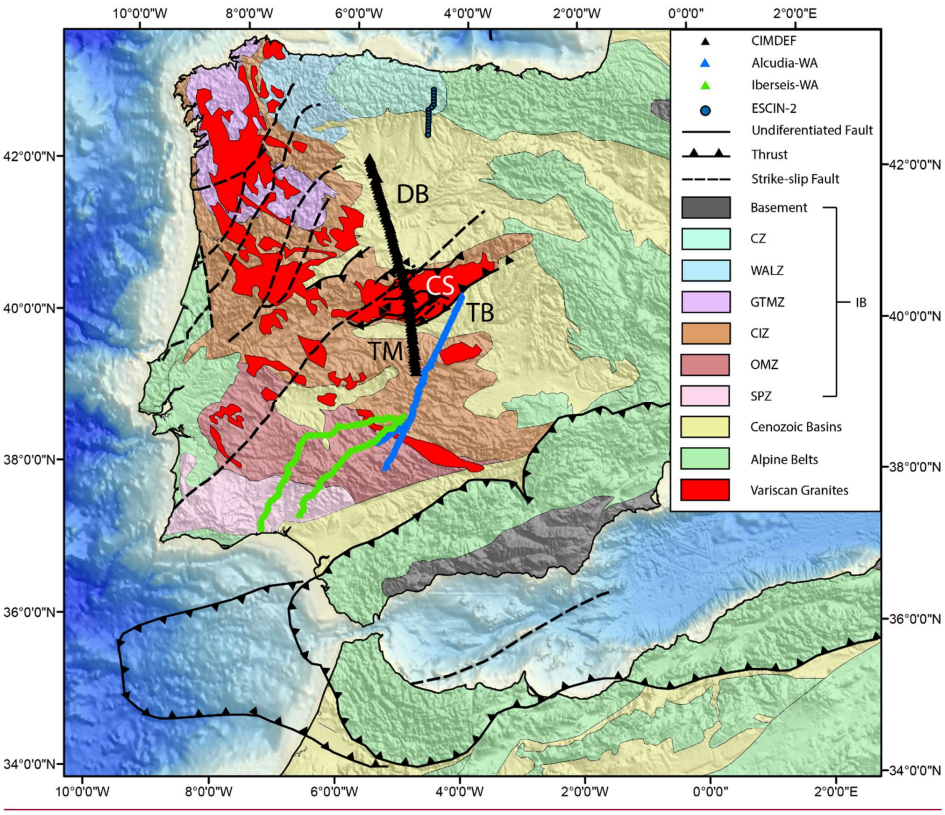
10°0'0"W
8°0'0"W
6°0'0"W
4°0'0"W
2°0'0"W
0°0'0"
2°0'0"E
42°0'0"N
40°0'0"N
38°0'0"N
36°0'0"N
34°0'0"N
DB
CS
TB
TM
CIMDEF
Alcudia-WA
Iberseis-WA
ESCIN-2
Undiferentiated Fault
Thrust
Strike-slip Fault
Basement
CZ
WALZ
GTMZ
CIZ
OMZ
SPZ
IB
Cenozoic Basins
Alpine Belts
Variscan Granites

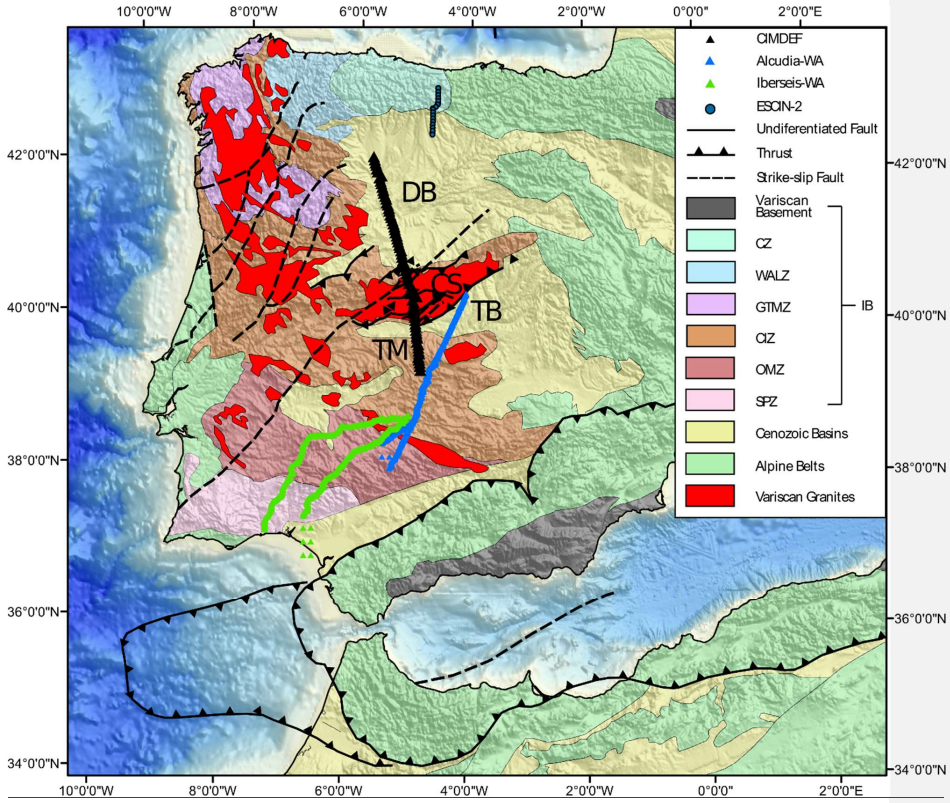

Figure 1. Simplified geological map of the study area with major tectonic provinces of the Iberian Massif and structures. TM: Toledo Mountains, CS: Central System, DB: Duero Basin, TB: Tajo Basin, CZ: Cantabrian Zone, WALZ: West-Asturian Leonese Zone, GTMZ: Galicia Tras-os Montes, CIZ: Central Iberian Zone, OMZ: Ossa-Morena Zone, SPZ: South Portuguese Zone. Location of granitoids is taken from Simancas et al. (2013).

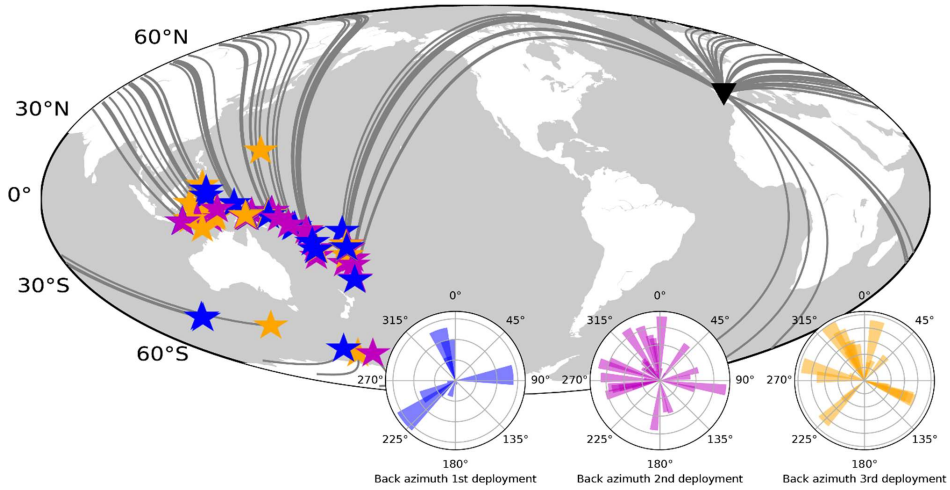

Figure 2. Colour-coded earthquakes (Magnitude ≥ 5) used for the three deployments. 17 earthquakes (blue stars) used for the central deployment, 38 (purple stars) for the southern, segment and 26 (orange stars) for the northern part of the profile. Polar plots represent the back azimuth of selected earthquakes for each deployment.

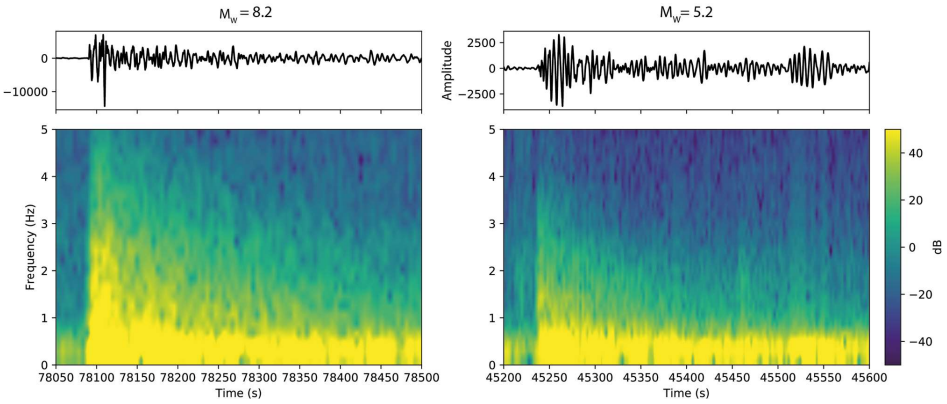

Figure 3. Power-spectral density of two earthquakes recorded by the CIMDEF array. They cover both ends of the used magnitudes, thus proving the existence of energy at the selected frequency band.

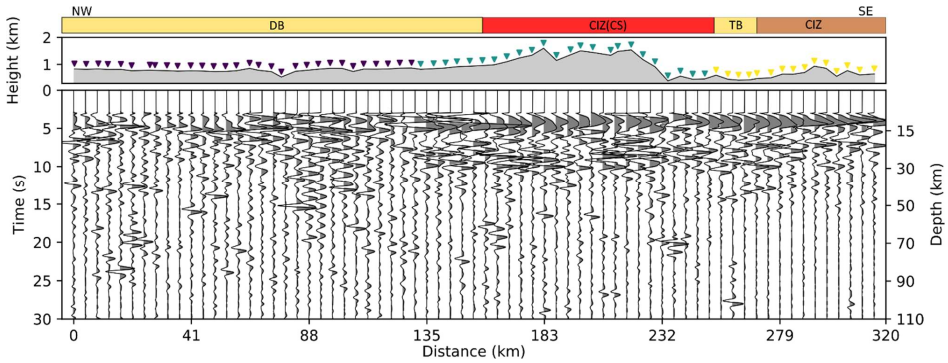

Figure 4. Reflectivity profile retrieved by Global-Phase Seismic Interferometry. In the wiggle plot, the grey lobes indicate positive polarity. On top, extend of the geological areas crossed by the profile. Coloured tringles represent the different acquisition stages (from north to South, 3rd, 1st, and 2nd deployments)

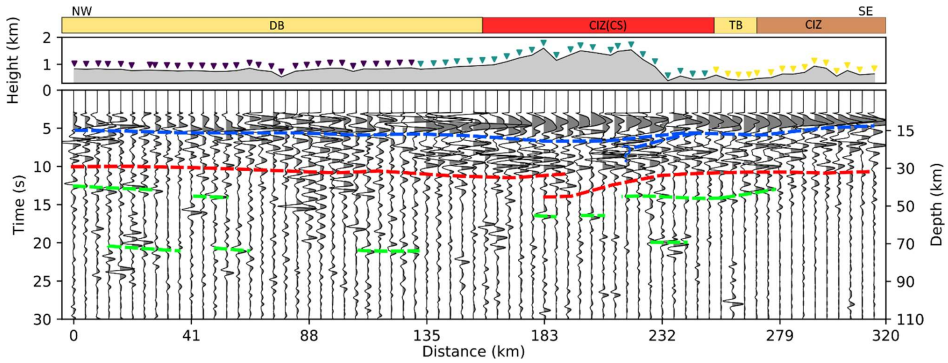

Figure. 5 Interpretation of the lithospheric reflectivity profile. The blue dashed line marks the boundary between the upper crust and the mid-lower crust. The red dashed line is the crust-mantle boundary. Scattered reflectivity within the upper mantle is marked by the green dashed lines.

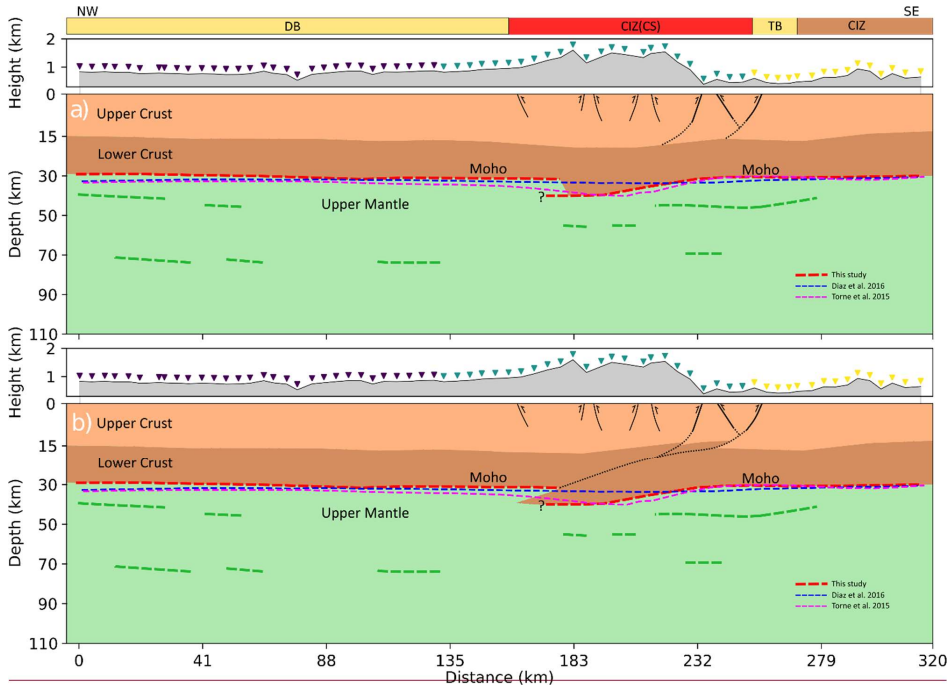
NW
SE
DB
CIZ(CS)
TB
CIZ
Height (km)
Depth (km)
a)
b)
Upper Crust
Lower Crust
Moho
Upper Mantle
This study
Diaz et al. 2016
Torne et al. 2015
0
41
88
135
183
232
279
320
Distance (km)

1235

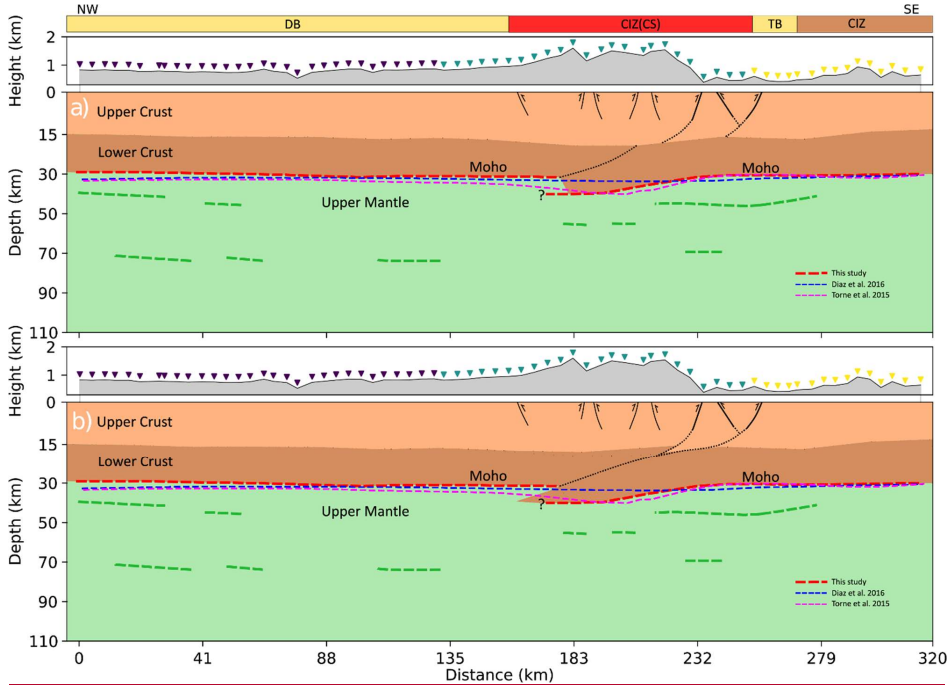
NW
SE
DB
CIZ(CS)
TB
CIZ
Height (km)
Depth (km)
a)
b)
Upper Crust
Lower Crust
Moho
Upper Mantle
This study
Diaz et al. 2016
Torne et al. 2015
0
41
88
135
183
232
279
320
Distance (km)

Figure. 6 Sketch of the proposed crustal geometry, overlapped with Moho results from gravity inversion and RF. a) model where the S thrust and the Tietar fault lie within the upper crust and only the lower crust imbricates; b) model where the entire crust imbricates below the CS

1240

1245

1250

Table 1. Global earthquakes used in this study.

Date	Latitude (º)	Longitude (º)	Depth (km)	Magnitude	Deployment
24/05/2017	-10.0191	161.9535	52	5.5	Central
25/05/2017	-22.3132	-176.3299	127	5.6	Central
29/05/2017	-1.2923	120.4313	12	6.6	Central
30/05/2017	-12.113	167.266	257.42	5.2	Central
02/06/2017	-4.7348	145.1363	192.85	5.9	Central
03/06/2017	-62.5792	155.834	10	5.9	Central
09/06/2017	-16.855	-177.6	10	5.6	Central
09/06/2017	5.486	125.139	13.99	5.2	Central
09/06/2017	-10.26	161.185	53.2	5.2	Central
10/06/2017	-54.3039	-146.639	10	5.6	Central
10/06/2017	-11.503	166.433	48.46	5.1	Central
12/06/2017	3.69	126.776	56.82	5.4	Central
14/06/2017	-18.3246	168.728	13.6	5.8	Central
15/06/2017	-30.5156	-178.0563	34	6	Central
15/06/2017	-55.414	-124.789	10	5.8	Central
17/06/2017	-24.0927	179.6041	511	6.1	Central
17/06/2017	51.76	-173.371	29.46	5.3	Central
25/02/2018	-6.0699	142.7536	25.21	7.5	South
25/02/2018	-5.8339	142.263	10	5.7	South
26/02/2018	-5.4592	151.8089	20.16	5.6	South

26/02/2018	-6.3991	143.2581	9	5.9	South
26/02/2018	-6.4973	143.5497	22	5.8	South
26/02/2018	-2.7774	126.6859	9	6.1	South
26/02/2018	-6.5052	143.255	19	6.3	South
27/02/2018	-18.8679	169.2903	203	5.5	South
27/02/2018	-6.4033	143.0332	12	5.7	South
27/02/2018	-60.2494	150.7793	10	6.1	South
28/02/2018	-6.1696	142.4681	16	6.1	South
02/03/2018	-6.1353	130.2782	135	5.9	South
04/03/2018	-6.0741	142.7211	6	5.7	South
04/03/2018	-6.331	142.5994	10	6	South
06/03/2018	-6.2314	142.4131	10	5.5	South
06/03/2018	-6.3043	142.6116	20.49	6.7	South
07/03/2018	-5.4456	151.3913	50	5.6	South
08/03/2018	-3.3428	130.9337	10	5.6	South
08/03/2018	-4.3762	153.1996	22.86	6.8	South
09/03/2018	-4.2814	153.3875	30	5.8	South
09/03/2018	-21.0006	-178.606	540.34	5.7	South
12/03/2018	-46.3559	95.9296	10	5.6	South
22/03/2018	-30.1742	-177.7218	22.22	5.5	South
24/03/2018	-5.4959	151.4971	33	6.3	South
24/03/2018	-45.7783	96.0692	10	6	South
25/03/2018	-7.3049	128.4848	144	5.7	South
25/03/2018	-6.6343	129.8172	169	6.4	South
26/03/2018	-5.5024	151.4025	40	6.7	South
29/03/2018	-9.4211	159.5792	32	5.8	South
29/03/2018	-5.5321	151.4999	35	6.9	South
29/03/2018	-5.899	151.8542	10	5.7	South
02/04/2018	-24.719	-176.8865	92	6.1	South
05/04/2018	-18.2946	-177.9138	511	5.8	South
06/04/2018	-1.4171	138.2026	10	5.6	South
07/04/2018	-6.3608	142.6662	10	5.5	South
07/04/2018	-5.8382	142.5314	18.07	6.3	South
15/04/2018	1.4083	126.8759	34	6	South
17/04/2018	-3.5216	131.3032	10	5.5	South
06/07/2018	-49.6301	126.0404	10	5.5	North
07/07/2018	-30.5662	-178.0701	35	6	North
08/07/2018	-21.2766	168.4961	10	5.5	North
08/07/2018	-19.0182	169.4901	255	5.5	North
13/07/2018	-18.9279	169.0467	167	6.4	North
17/07/2018	-11.5936	166.432	37.96	6	North
20/07/2018	18.45	145.993	121	5.6	North
22/07/2018	-18.9577	168.8868	103.46	5.5	North
28/07/2018	-7.1039	122.7263	578.16	6	North
28/07/2018	-8.2395	116.508	14	6.4	North
05/08/2018	-8.2579	116.4403	34	6.9	North
10/08/2018	-62.6208	165.635	10	5.6	North
17/08/2018	-7.3718	119.8017	529	6.5	North

19/08/2018	-18.1132	-178.1523	600	8.2	North
19/08/2018	-18.4447	-177.6404	575.76	6.3	North
19/08/2018	-18.2293	-178.1002	537.63	5.6	North
19/08/2018	-18.2748	-178.3539	618.29	5.7	North
19/08/2018	-8.3366	116.5993	16	6.3	North
19/08/2018	-16.9783	-178.0332	415.6	6.8	North
19/08/2018	-8.319	116.6271	21	6.9	North
19/08/2018	-8.3511	116.5565	10	5.8	North
20/08/2018	-18.1559	-178.1888	526.17	5.5	North
21/08/2018	-16.0295	168.145	9	6.5	North
22/08/2018	-6.9675	155.7284	34	5.8	North
28/08/2018	-10.8859	124.1187	14	6.2	North
28/08/2018	-18.0299	-177.9387	600.62	5.7	North

1255